NASA CR-112264

THE APPLICATION OF GENERAL AERODYNAMIC LIFTING SURFACE ELEMENTS TO PROBLEMS IN UNSTEADY TRANSONIC FLOW

BY
ATLEE M. CUNNINGHAM, JR.

FEBRUARY 1973

PREPARED UNDER CONTRACT NAS1-11565

BY

GENERAL DYNAMICS
CONVAIR AEROSPACE DIVISION
P. O. BOX 748
FORT WORTH, TEXAS 76101

FOR

NATIONAL AERONAUTICS AND SPACE ADMINISTRATION

THE APPLICATION OF GENERAL AERODYNAMIC LIFTING SURFACE ELEMENTS TO PROBLEMS IN UNSTEADY TRANSONIC FLOW

by

Atlee M. Cunningham, Jr.

ABSTRACT

A study is conducted to investigate the feasibility of using combined subsonic and supersonic linear theory as a means for solving unsteady transonic flow problems in an economical and yet realistic manner. With some modification, existing linear theory methods are combined into a single program and a simple algorithm is derived for determining interference between lifting surface elements of different Mach number. The method is applied to a wide variety of problems for which measured unsteady pressure distributions and Mach number distributions are available. By comparing theory and experiment, the transonic method solutions show a significant improvement over uniform flow solutions. As a result of studying the experimental data, several areas of further research are suggested for refining the method. It is concluded that with these refinements the method will provide a means for performing realistic transonic flutter and dynamic response analyses at costs which are compatible with current linear theory based solutions.

TABLE OF CONTENTS

TABLE OF CONTENTS (CONTINUED)

NOMENCLATURE

Symbols

a	Speed of sound, meters/second
$\bar{a}$	Conical coordinate
AR	Aspect ratio
B	Supersonic Prandtl-Glauert factor, $B^2 = M^2 - 1$
b_{REF}	Reference length, meters - usually ½ wing chord for 2-dimensional flow or ½ MAC for finite wings in 3-dimensional flow
c	Wing chord, meters
C_L	Lift coefficient
C_m	Moment coefficient
C_p	Pressure coefficient, $\frac{p-p_\infty}{q_\infty}$
$D(x)$	Unit step function = 1, $x \geq 0$ = 0, $x < 0$
$h(x,y)$	Mode amplitude at point x,y, meters
i	$\sqrt{-1}$
k	Reduced frequency = $\frac{\omega b_{REF}}{U}$
M	Mach number = $\frac{U}{a}$
MAC	Mean aerodynamic chord, meters
p	Pressure, Newtons/meter^2
q	Dynamic pressure = $\frac{\rho U^2}{2}$ Newtons/meter^2
r	$\left[(y-\eta)^2 + (z-\zeta)^2 \right]^{\frac{1}{2}}$, meters
s_o	Wing semi-span, meters

Symbols

U_∞	Free stream velocity, meters/second
u,v,w	Velocity components in the x,y,z directions, respectively, meters/second
x,y,z	Cartesian coordinate location of the downwash point in the kernel function (x is in the direction of U_∞), meters
x_o, y_o, z_o	Distance from an influence point to the downwash point, $(x-\xi)$, $(y-\eta)$, $(z-\zeta)$, meters
x,y,z	$\left(\frac{x}{b_{REF}}\right)$, $\left(\frac{y}{b_{REF}}\right)$, $\left(\frac{z}{b_{REF}}\right)$
ΔC_p	Lifting pressure coefficient
α	Angle of attack, degrees
β	Subsonic Prandtl-Glauert factor, $\beta^2 = 1-M^2$
ξ, η, ζ	Location of an influence (or integration) point in the kernel function, meters
$\bar{\eta}$	$\frac{\eta}{s_o}$
ω	Rotational frequency, radians/second

Subscripts

ı	Local conditions
LE	Leading edge
MC	Mach cone (or hyperbola) boundary
TE	Trailing edge
xy	Local value at point x,y
∞	Free stream conditions

INTRODUCTION

In recent years, interest has grown considerably in the desire to fly efficiently in the high subsonic regime as indicated by various Government sponsored transonic research programs such as ATT, F-111 TACT and others. As a result, the need has increased for better unsteady transonic aerodynamic tools so that flutter and dynamic response characteristics can be more accurately predicted in this flow regime. Presently, for lack of anything better, these characteristics are predicted only with methods which are based on linearized theory in uniform potential flow. In addition, since buffet and limit cycle flutter appear to be similar in experimental flutter and buffet testing, it is important that their distinction be better understood.

The characteristic of transonic flow which causes the greatest difficulty when attempting to apply uniform flow theory to such problems is the presence of shocks imbeded in the flow. Clearly, such a gradient in velocity as that which exists across a shock is no longer small, thus, linear theory cannot account for this phenomenon and hence becomes invalid. Finite difference methods or other iterative schemes can account for such discontinuities but they are usually very expensive to use in terms of computer time required. Moreover,

if they are used for flutter or dynamic response analyses where solutions must be computed for 10 or more frequencies, the computer costs quickly become astronomical. For example, a simple cantilevered wing flutter analysis with four natural modes and 10 frequencies could require 20 or more hours of computer time for a single flutter solution. Thus, such an approach is not well suited for solving unsteady transonic aerodynamic problems in a practical sense.

This report presents the results of a study conducted to investigate the feasibility of using combined subsonic and supersonic linear theory as a means for solving unsteady transonic flow problems economically. In the method developed, a wing over which the flow is mixed supersonic and subsonic with imbedded shocks is treated as an array of multiple lifting surfaces. Each surface is allowed to have mutual interference with the other surfaces. Also, each is assigned a different Mach number, either subsonic or supersonic, and its downwash is modified accordingly. In order to determine the Mach number distribution and shock geometry, information is first needed from either experiment or a finite difference solution, hence the method is used to predict unsteady perturbations about known steady mean flows.

With planform and flow geometry established, the configuration is assembled with general aerodynamic lifting surface (GALS) elements, for which each is assigned a mean Mach number, Mach number distribution, aerodynamic control point array, and boundary conditions. The solution proceeds from this point in a manner identical to ordinary aerodynamic interference methods[1]. The frequency sweep can be performed at about the usual cost of a standard subsonic or supersonic unsteady aerodynamic analysis which is less than one hour - usually about 10 minutes - as opposed to 20 hours or more for a finite difference solution.

TRANSONIC FLUTTER AND DYNAMIC RESPONSE ANALYSIS

The final objective of this research in unsteady transonic flow is the development of a method for predicting flutter and dynamic response characteristics of general aerodynamic configurations. It is therefore appropriate that a brief discussion be given at this point concerning the problems associated with transonic flutter and dynamic response analysis. This discussion will consider the differences between transonic and uniform flow analyses, transonic methods available, economics of the problem, and a practical method for solution.

The Differences Between Transonic and Uniform Flow Analysis

In the past (and present), the Mach-altitude envelope over which the configuration was to be shown to be flutter free posed no serious problems from a computational standpoint. Since the analysis methods were linear, there was no coupling between the unsteady aerodynamics and altitude save for a simple multiplicative factor which contained the density of the air. Also, there was no effect due to mean angle of attack, camber, twist, or thickness. In transonic flow, this is no longer true.

In order to be realistic, a transonic method must account for several characteristics which were previously ignored as mentioned above. The prediction of unsteady pressure distributions induced by an oscillating surface in mixed transonic flow is complicated by the strong coupling between the steady and unsteady flow fields. The steady flow fields are in turn drastically modified by Mach number, altitude, thickness, camber, twist, angle of attack, interference, and boundary layer effects. Unlike pure subsonic or supersonic flow, these effects are no longer second order and hence cannot be ignored.

Effects of thickness and camber may be lumped under airfoil geometry effects which function to locate a normal shock on the upper and lower surfaces in the two-dimensional case of supercritical flow. Symmetric non-cambered airfoils at zero angle of attack will show the same shock location on both surfaces. Non-symmetric airfoils such as supercritical and lifting airfoils with camber and/or angle of attack, will show different shock locations on the upper and lower surfaces. At high enough positive angles of attack, the shock on the lower surface may even disappear depending on the Mach number.

For three-dimensional flow, in addition to airfoil geometry effects, planform geometry, twist, and interference effects must be considered. Their primary function is to define the shock structure over the entire configuration on both upper and lower surfaces. The shock structure will vary with any of these quantities; however, for a fixed configuration, the only geometric variable remaining is the angle of attack, α .

Altitude is no longer a simple variable in transonic flow. Its influence is felt through the Reynold's number effects on the shock-boundary-layer interaction. These interactions are somewhat unique in that they affect both steady and unsteady forces. The effect on the steady mean flow is to modify the shock structure as determined by the configuration geometry through the effective thickness increment due to the boundary layer. The unsteady forces induced by the interactions are due to shock oscillation and shock induced separation. These unsteady forces are those that are normally referred to as transonic buffet forces.

As a result of the above discussion, it is clear that transonic flutter and dynamic response analyses must be performed over a three-dimensional envelope as specified by the Mach-altitude-α conditions. What further complicates the problem is that the entire configuration, upper and lower surfaces, must be considered in almost all cases.

Through changes in the boundary layer, altitude affects the entire shock structure as well as does Mach number and α . Thus, a new shock geometry is necessary for each Mach-altitude-α condition. It is now apparent that an economical means for predicting unsteady transonic aerodynamic loads is mandatory before a realistic flutter and dynamic response capability can become a reality.

Available Transonic Methods

For a transonic method to be practical, the input data requirements should be minimal without restricting the method's capability. Thus, one should be able to simply supply the configuration geometry, natural mode shapes, Mach, altitude, and α data to a computer procedure that would solve the problem in a manner which accounted for all of the effects above. With the present state-of-the-art, such a capability is either impossible to achieve or if it is available in the near future, it will be too expensive to be practical for dynamics problems. On the other hand, the blind application of linearized uniform potential flow theory to transonic problems leaves much to be desired and any step in the right direction would be an improvement.

For lack of anything better, conventional transonic flutter analysis has been performed by bracketing the forbidden zone with subsonic ($M_\infty \leq 0.95$) and supersonic ($M_\infty \geq 1.2$) linear solutions and then fairing through the range $0.95 < M_\infty > 1.2$. Runyan and Woolston[2] approached the problem with the subsonic kernel function by taking the limit as $M_\infty \rightarrow 1.0$. This did not account for mixed flow or any of the effects discussed previously. Methods have also been developed specifically for $M_\infty = 1.0$ flow[3,4] which are subject to the same restrictions. The unsteady transonic box method developed by Rodemich and Andrew[3] was demonstrated by Olsen[5] to agree only qualitatively with experiment. The comparison was clouded by uncertainty in the experimental data. This method was later modified by Stenton and Andrew[4] to include swept trailing edges and trailing edge control surfaces. However, the approach was not altered. Because these methods cannot account for transonic characteristics in a realistic manner, they are not practical.

Methods are available for steady flow which provide a more realistic treatment of transonic flows. The method of Magnus and Yoshihara[6] uses a time dependent finite difference solution to the compressible unsteady Euler equations. It is applicable to thick and blunt airfoils in steady flow and it can be readily extended to unsteady flow. Viscous effects

cannot be considered without resorting to some type of artificial scheme which involves approximation of the boundary layers. The method of Murman and Cole[7] can be adapted to unsteady flow by including the unsteady terms in the non-linear small perturbation potential equation for transonic flow. This method is also inviscid but it cannot be applied to thick, blunt airfoils due to restrictions imposed by the small perturbation equation. Neither of these methods have three-dimensional capability and their cost per solution is extremely high compared to the linear theory methods. Extension to three-dimensional flow will result in even more costly solutions unless they are modified to improve speed of convergence or relax grid requirements.

If one could disregard economy, clearly methods based on a finite difference or relaxation scheme would be the most practical since they can better account for the transonic effects. If economy was the driving factor and accuracy secondary, then the linearized transonic solutions would be the better choice. Since neither economy nor accuracy can be ignored, the best approach would be to combine the advantages of both and eliminate the disadvantages as much as possible.

Economics of Transonic Unsteady Aerodynamics

A discussion of economy of solution is meaningless unless the cost is compared with other aspects of the design process. In order to appreciate the economic impact of a finite difference flutter analysis on an IBM 360/65, a simple flutter problem will be considered.

The problem will be to perform a flutter analysis on a simple cantilevered wing of trapezoidal planform in mixed transonic flow. The first four natural modes will be used and generalized aerodynamic force matrices will be computed at 10 frequencies. These matrices will be interpolated at other frequencies between the set of 10 and the resulting flutter determinants solved for the modal damping and natural frequency as a function of velocity. The damping and frequency values are plotted on a V-g (velocity-damping) diagram which is used to define the root loci for each mode. Flutter is defined at the velocity where damping of one of the modes becomes positive.

Considering a linear theory solution (kernel function method), it will be assumed that solution time would be about 0.5 to 1.0 minute per frequency. Since a well designed linear theory method uses the inverted aerodynamic matrix, the cost for multiple mode solutions is no more than that for a matrix-vector multiplication. Thus, once the inverted matrices

are obtained, they can be used repeatedly for subsequent problems at very little cost. The cost for 10 frequencies is then 5 to 10 minutes of computer time for a single flutter solution on an IBM 360/65. (The cost of interpolation, assembling the flutter determinants, and flutter solution are not considered since they are usually small compared to the aerodynamic solution.)

Although it is not possible to predict the computer run time for an unsteady three-dimensional finite difference or relaxation solution at this time, an idea can be derived from the results obtained by Bailey and Steger[8]. Their hybrid method for steady flow combines the small perturbation equations for velocity components and velocity potentials to solve lifting cases in mixed transonic flow. The method is applicable to finite wings of swept or non-swept rectangular planform but not to thick or blunt airfoil sections. Computer times for finite wing solutions ranged from 30 to 60 minutes on an IBM 360/67. The total iterations required for convergence was not greatly increased in going from two-dimensional to three-dimensional solutions; however, a greater number of grid points was needed thereby raising the solution cost. The number of iterations (and hence computer time) did increase with increasing transonic effects and grid refinement.

Based on the above discussion, it may be assumed that a single finite difference solution for a finite wing in steady or unsteady flow would take about 30 to 60 minutes on an IBM 360/65. Since a solution must be obtained independently for each mode shape, then the total number of aerodynamic solutions necessary for a single flutter analysis would be 4x10=40. Thus, 20 to 40 hours of computer time on an IBM 360/65 would be required for one flutter analysis.

Returning to the previous discussion on transonic flutter analysis, the envelope is three-dimensional as defined by the Mach-altitude-α conditions. For two Mach numbers, two altitudes, and two α's, the total cost of a "linear theory transonic flutter analysis" would be from 40 to 80 minutes. Redesign evaluations with new modes would cost about 8 minutes per mode set. The finite difference analysis would cost from 160 to 320 hours on the IBM 360/65 for the Mach-altitude-α conditions. Moreover, redesign evaluations would cost the same if the new modes changed substantially as they often do.

In this example, the use of a finite difference flutter analysis method would result in a cost in computer time which was equivalent in dollars to the order of magnitude cost of a flutter model test program for the simple cantilevered trapezoidal wing. Also, routinely tying up a computer for

20 to 40 hours becomes an impractical situation in a typical industrial computing facility. Since one of the primary objectives for using theoretical flutter methods is to reduce costs by minimizing the requirement of flutter model tests, then it seems that the finite difference approach is defeating its intended purpose. Thus, attention will now be turned to combining the methods.

The Hybrid Approach to Unsteady Transonic Flow

A practical method for flutter and dynamic response analysis in transonic flow must be realistic, reliable, and feasibly economical. In order to be realistic, the method must account for mixed flow with imbedded shocks as characterized by transonic flows. The second requirement means that reliable and consistent results can be obtained without a lot of "hand waving" or "data juggling". The results must yield valid trend data for design variations. Finally, the method must be able to predict these characteristics within the budget limitations imposed by the development program in which it is being used. Thus, a balance must be maintained between desired accuracy and available budget.

Two facts are known about transonic flow which provide some guidance for developing a practical approach. First, most of the non-linear effects associated with variations in Mach-altitude-α conditions are manifested in the steady mean flow. Second, the oscillatory forces needed for flutter and dynamic response analysis are usually small compared to the steady mean forces.

The steady mean flow characteristics can be obtained in two ways. The finite difference or relaxation schemes discussed previously can be used to define the mean flows for the Mach-altitude-α conditions required. Since these methods are presently very limited in capability, further development is needed in this area. Another way is to use measured pressure distributions from wind tunnel data which is usually available in a typical configuration development program.

The oscillatory perturbations should be obtained with a method that operates like the linear theory methods with inverted aerodynamic matrices. The method which is the subject of this report is such a method. It uses general aerodynamic lifting surface (GALS) elements which can represent a mixed subsonic-supersonic flow field with linear theory solutions[9]. By knowing the steady mean flow field in advance, the general aerodynamic elements can be arranged to fit shock and planform

geometries to practically any degree desired. The method is basically an interference kernel function method whose run time per matrix is proportional to the number of aerodynamic control points (or unknown pressure functions).

Application of the hybrid approach to the cantilevered wing problem would require 8 finite difference solutions for the Mach-altitude-α conditions or a total of 4 to 8 hours of computer time. In addition, 10 oscillatory solutions with the GALS element method would be required at each condition. The cost per frequency would be about 1 minute (as will be shown later in the report); thus, the total would be 8x10x1=80 minutes or 1 1/3 hours for the oscillatory forces. Finally the combined cost for the hybrid analysis would be 5 1/3 to 9 1/3 hours on the IBM 360/65 as compared to 160 to 320 hours for a pure finite difference analysis. Subsequent analyses for each new set of mode shapes would require about 8 minutes. This approach best fits the three requirements set forth for a practical method.

The remainder of this report will be concerned with the use of the GALS element method to predict unsteady pressure distributions on wings oscillating in mixed transonic flow fields with imbedded shocks. The modes of oscillation and planform geometry are arbitrary and interference is permitted.

TRANSONIC CHARACTERISTICS - A DESCRIPTION OF THE PROBLEM

Before proceeding with discussion of the method for solving the unsteady mixed-flow transonic aerodynamic problem, some description of observations made on experimental results is in order. Basically, these are separated into two groups: steady or low frequency characteristics and unsteady or high frequency characteristics. The primary purpose of this section is to provide insight to the problem which facilitates understanding of what must be predicted and perhaps how it may be predicted.

Steady or Low Frequency Characteristics

One of the best known transonic characteristics in steady flow is the so called "glich" in the lift curve which occurs at medium high angles of attack at high subsonic Mach numbers. In Figure 1, a hypothetical example is shown for the lift curve "glich". The occurrence of this phenomenon has been tied to the passing of the shock on the upper surface over the local crest as prescribed by the angle of attack. What is believed to happen is that since the upper shock is not stable on the crest, it suddenly moves from just behind to just in front of the crest for a very small increase in angle of attack. The

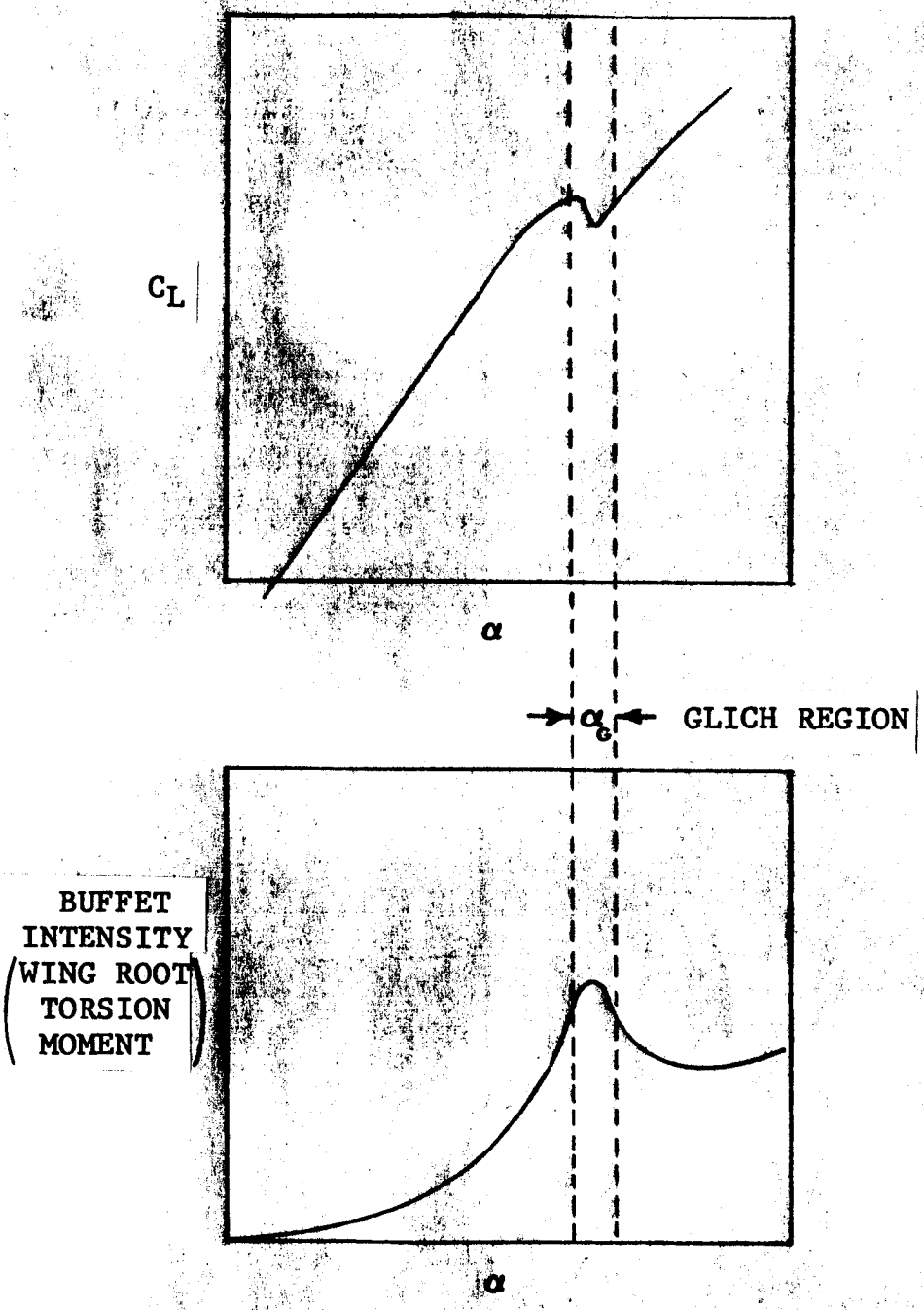

Figure 1 HYPOTHETICAL TRANSONIC GLICH CHARACTERISTIS

17

lift gain for the small angle increase is almost zero whereas the lift loss due to the increase in the area of high pressure behind the shock on the upper surface is sizable. The result is a net loss in lift due to a small increase in angle of attack, and hence a "glich" or a negative slope occurs in the lift curve. Because of the unstable nature of the shock near the crest, the "glich" region has also been shown to be a region of maximum buffet intensity. After the glich is cleared and the shock is in a stable position forward of the crest, the buffet intensity drops as is indicated by the second curve in Figure 1. The next peak in buffet intensity does not occur until the flow becomes separated from the leading edge.

The significance of the negative lift curve slope is that low frequency torsional motion at angles of attack near the glich angle, α_G, creates aerodynamic forces on the upper surface that are 180^o out of phase with the motion. The amplitude, however, is almost independent of the oscillatory increment of α due to the torsional mode. The lower surface on the otherhand, sees the more conventional aerodynamic force due to torsional motion which is nearly in phase with the mode at low values of reduced frequency. In addition to its phasing, the lower surface force is much more amplitude dependent than that on the upper surface due to shock motion about the crest.

Hence, with the upper surface pressures acting as a nearly constant amplitude driving force, the amplitude of the motion must increase such that the upper and lower forces cancel each other in an equilibrium motion. Thus, a limit cycle one degree of freedom flutter condition, commonly called transonic buffet, can occur in this manner. The occurrence of this torsional mechanism has been observed as a peak in oscillatory torsional pivot moment near the lift curve glich in the F-111 1/6-scale model tests conducted at NASA Ames Research Center.

Although it is beyond the scope of the present study to predict the shock motion induced forces due to the shock instability as it passes the crest, the phase relationship between forces due to shock motion and surface movement is a fundamental characteristic of mixed transonic flow. Figure 2 shows the steady upper and lower surface pressures at midspan on the rectangular wing at M_∞=0.90 as taken from TND-344[10]. The wing is at zero angle of attack, however, there is lift on the wing presumably due to flow angularity. The apparent inclination is nose down as indicated by the downward net lift on the forward 60%-70% of the surface. Aft of that point, the Mach number begins to decrease through a shock from a maximum of about 1.14 to the free stream value of 0.90 at the trailing edge. The important characteristics are that the

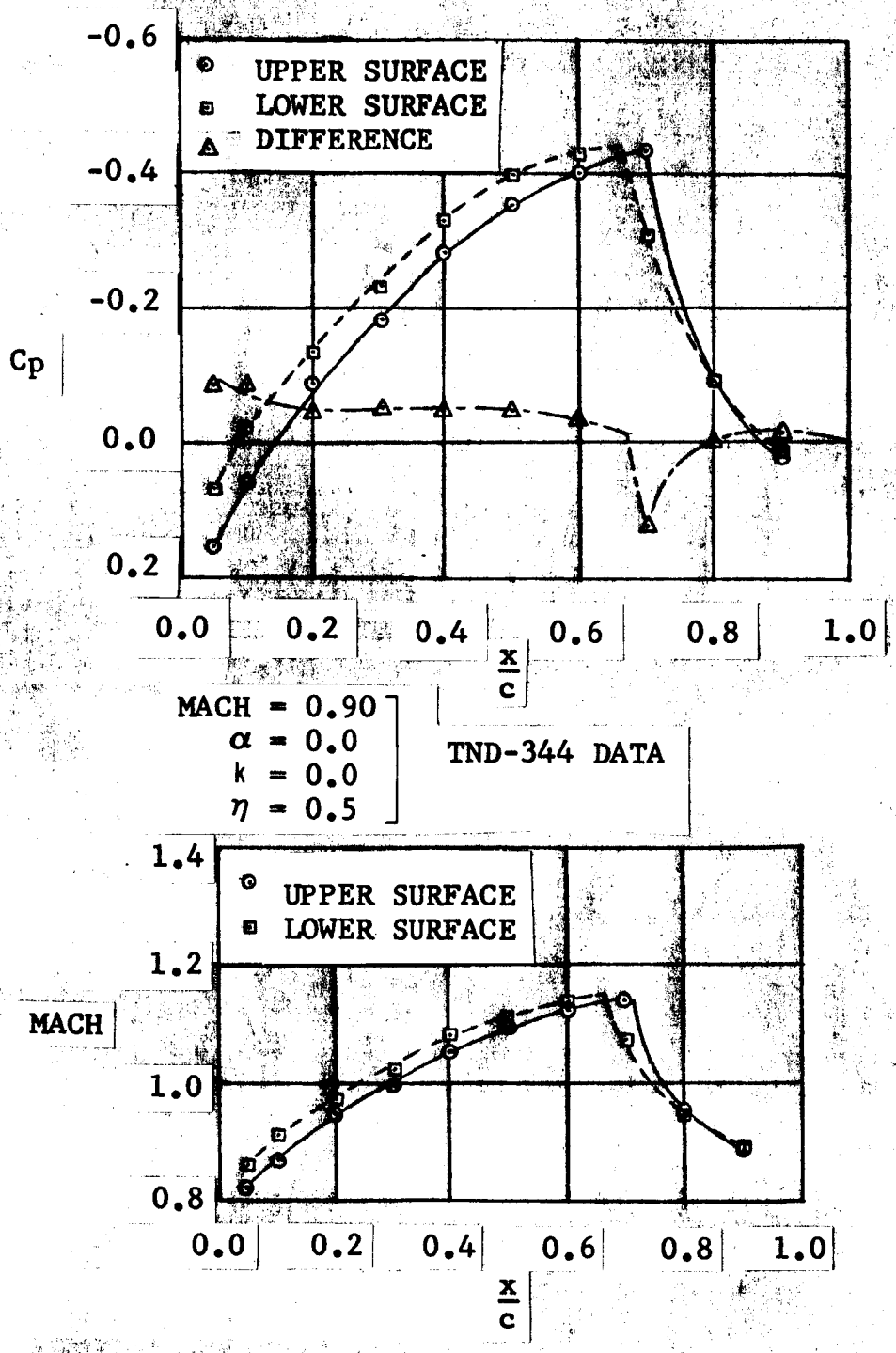

Figure 2 UPPER AND LOWER SURFACE PRESSURE AND MACH NUMBER VARIATION AT $\bar{\eta}$=0.5 ON A RECTANGULAR WING

20

maximum Mach number appears to be the same on the upper and lower surfaces and that the lifting forces behind the shock are in the opposite direction, or 180° out of phase. This property is carried over into the unsteady pressures at M_∞=0.90 for a low frequency (k_∞=0.13) bending mode oscillation also given in TND-344 for the α=0° case. (For the α=5° case, the upper surface is in separated flow, hence, its results are not too useful.) The nominal phase shift from in front to behind the shock is about +140° to +160° in the experimental data along the span. The same characteristic is also observed in some results obtained by Triebstein[11] on a rectangular wing oscillating in pitch at a low frequency (k_∞=0.138). These will be further discussed in the numerical examples.

Also shown in Figure 2 is the measured lift distribution which shows the peaking tendency in the vicinity of the shock. Thus, the main characteristics of steady or low frequency mixed transonic flows are the 180° phase shift and peak aft of the shock. The frequency must be zero or low enough to permit sufficient communication between the shock region and the trailing edge necessary to maintain the steady characteristics.

Unsteady or High Frequency Characteristics

The characteristics described above are modified considerably as the frequency increases. In this situation, the time lag required for wake disturbances to reach the shock is finite and constant for a given flow condition. Thus, the forward movement of the shock with a loss in pressure may not exist for high frequency flow.

In order to illustrate what may happen, let us consider a hypothetical shock which is situated such that it will never receive any signals from the wake, i.e., it sees only the local streamwise velocity perturbations. In this case, the load induced by shock motion changes entirely since the shock tends to move with the velocity perturbations. This type of movement is a result of the shock strength tendency to remain constant. Consider the velocity perturbations, Δu_1 forward and Δu_2 aft of a normal shock. If Δu_1 is about the same as Δu_2 and both are directed downstream (corresponding to a uniform drop in pressure), the Mach numbers, M_1 forward and M_2 aft of the shock, must both increase if the shock remains stationary. This will violate the shock relations and is hence inadmissible. The only way for a normal shock to remain in equilibrium is for it to move with Δu_1 and Δu_2 such that M_1 and M_2 satisfy the shock relationships. Since the velocity increments are not

equal, M_1 and M_2 will change slightly and the shock will move at some Δu_s which would be more of an average of Δu_1 and Δu_2. If the pressure is rising, Δu_1 and Δu_2 are directed upstream, hence, the shock will move forward in about the same manner. These shock motions are similar to those observed in engine inlet ducts during compressor surge or stall in supersonic flow.

The loading induced in the hypothetical case above may be explained through a simplified example. Considering the airfoil in Figure 3, the first step is shown in (a) where the velocity increment on the upper and lower surfaces is at a maximum. This corresponds to high pressure on the upper surface (forward Δu_{max}) and low pressure on the lower surface (aft Δu_{max}). In order to maintain the local absolute Mach number, the shocks must move with the local velocity perturbations on both the upper and lower surfaces. Hence, they will move in opposite directions. Continuing to (b), the mean value of pressure has been reached on both surfaces, hence, the shock movement stops. At this point, the lift increment due to shock displacement is downward as a result of the high pressure behind the shock. Thus, the shock induced loading lags the surface pressure loading by 90 degrees. In step (c), the low pressure peak on the upper surface (aft Δu_{max}) and high pressure peak on the lower surface (forward Δu_{max}) have been reached.

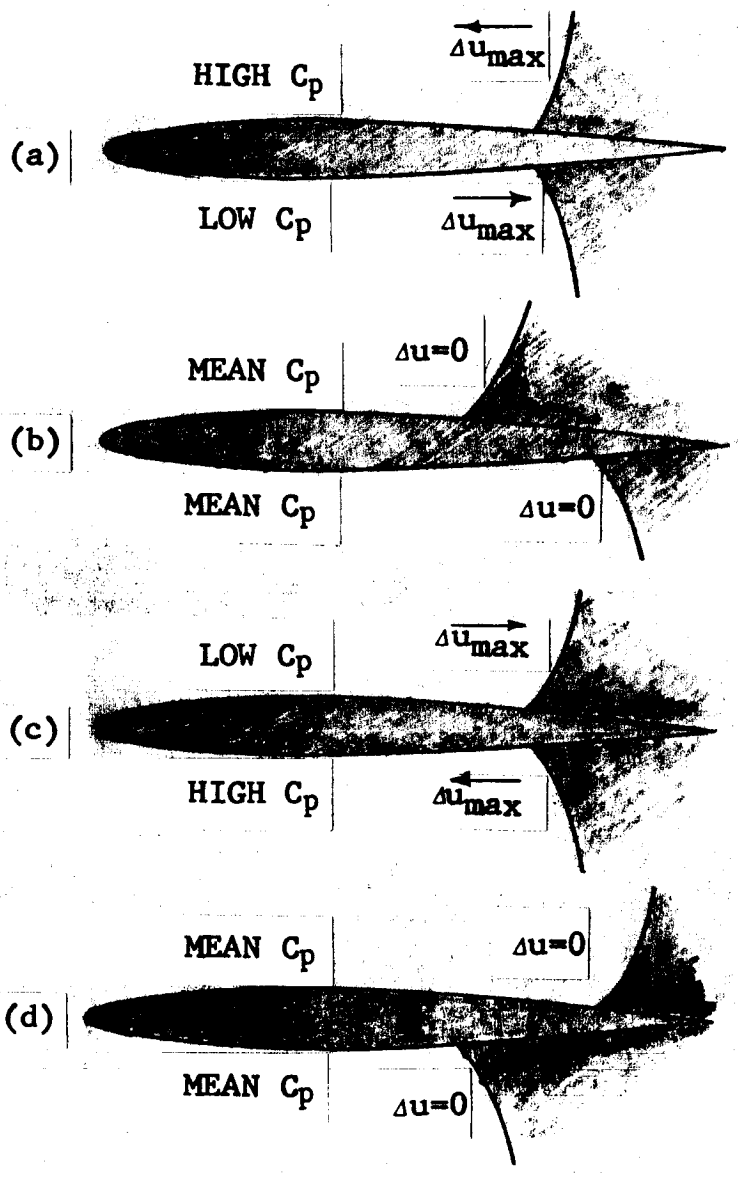

Figure 3 HYPOTHETICAL SHOCK MOVEMENT WITH LOCAL PRESSURE FLUCTUATIONS

27

At this point, the shocks are moving with maximum velocity and are again passing each other at the mean position but going in the opposite direction from that shown in step (a). Step (d) shows the maximum upward loading condition for shock motion where Δu has reached zero on both the upper and lower surfaces. At this point, the lower shock has moved to its forward most position and the upper shock has moved to its aft most position where again the shock motion induced lift is lagging by 90 degrees. If the upper and lower shocks do not have the same mean position, the same story is true; however, the shock movements will be different due to differences in the mean flow. The principal result will be an induced oscillatory moment as well as a lift component.

Returning to the real world, we now consider what happens when the wake signals are included. In low frequency or steady flow, sufficient time is available for the wake signals to propagate forward and "inform" the shock as to what the available final pressure is at the trailing edge. With a sudden drop in pressure on the upper surface, however, the shock initially moves aft in order to accommodate the change in local velocities as was discussed above. The drop in pressure is reflected from the trailing edge by pressures from the opposite surface which are experiencing a rise in amplitude. The

reflected wave is a compression wave which counteracts the expansion. When the compression wave meets the aft moving shock, it forces the shock to slow down or reverse its motion and move forward. In this situation, the transient case was considered. For "steady" oscillatory flow, the trailing edge signals will indicate a lagging phase angle which could be estimated in the same manner as discussed by Tijdeman and Bergh[12] for a control surface oscillating on an airfoil in two-dimensional flow. For the current problem, the time lag would be obtained for disturbances propagating from the trailing edge rather than the control surface hinge line as was done in Reference 12.

If the trailing edge signals are lagging by say 45 degrees at the shock, the pressure amplitude at the shock increases considerably. In Figure 4, the net pressure amplitude at the shock is shown for a hypothetical case in which the oscillating pressure at the shock due to local disturbances is assumed to be reacted by a trailing edge signal which is twice as large in amplitude and opposite in sign. The solid line represents what happens in quasi-steady flow where the trailing edge signal does not lag. The resultant in this case is an oscillatory pressure of equal amplitude but opposite sign compared to the pressures induced by local disturbances.

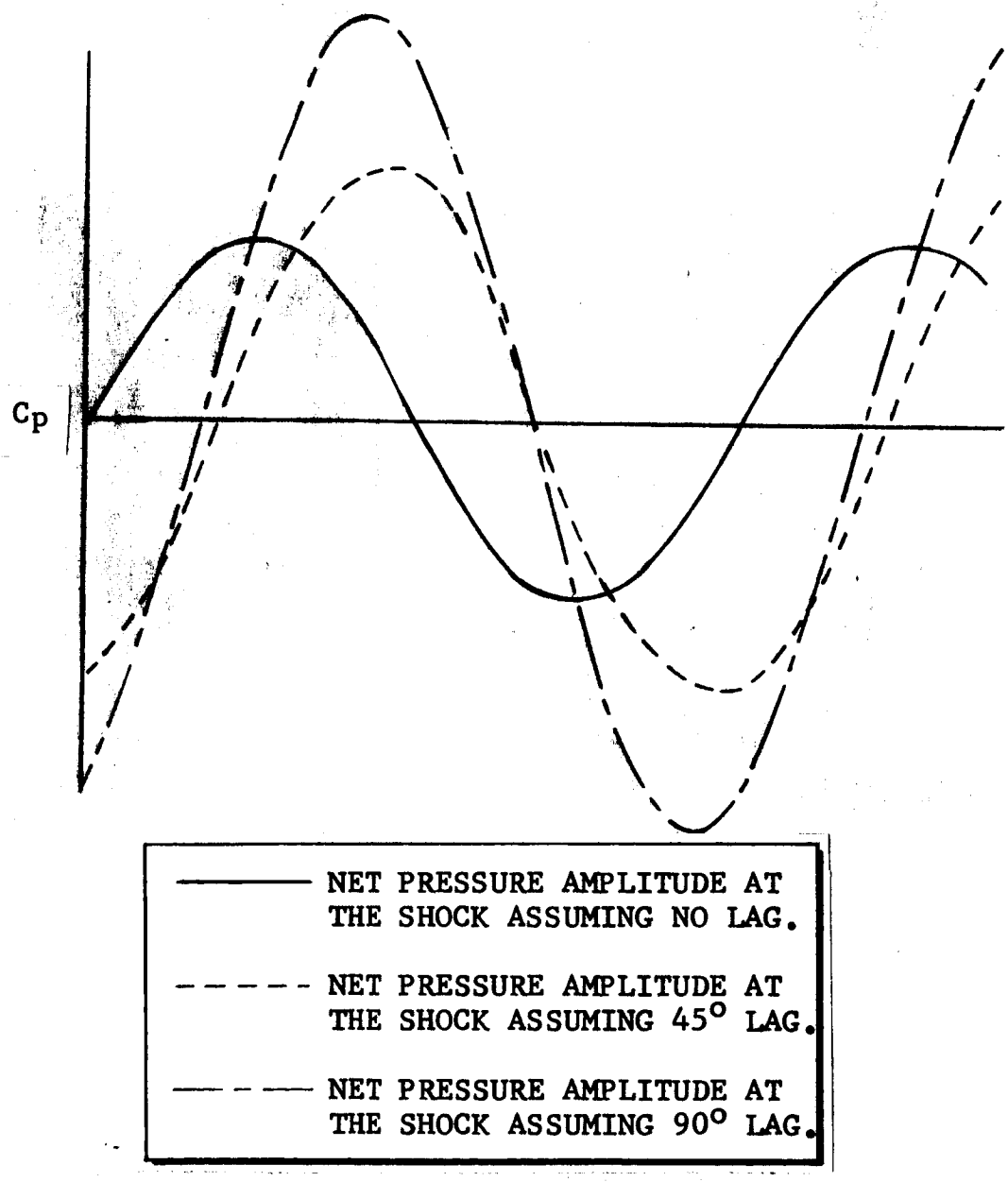

Figure 4 EFFECT OF WAKE SIGNAL LAG ON PRESSURE AMPLITUDE AT THE SHOCK

If the trailing edge signal lags by 45 degrees, the resultant is the long dashed line which shows a larger amplitude by about 50%. By increasing the lag to 90 degrees, as is shown by the short dashed line, the amplitude increases by about 125%. Of course, if the lag is 180 degrees, the amplitude is simply the sum of the curves which has an amplitude 200% higher than the local disturbance. (Note also the shift in phase angle.)

As a result of lag, assuming that the trailing edge signal is on the order of twice as large as the local disturbance, the shock oscillation should tend to increase with increasing lag. Thus, as the shock mean position moves aft with increasing free stream Mach number, it would be expected that the shock oscillation peak should diminish since the lag would decrease as the trailing edge is approached. This characteristic has been observed in experimental data and the trend is predictable as will be discussed later under "Applications of the Transonic Method."

If all disturbances originate downstream of the shock in the subsonic region, the characteristics are much simpler. The case of an oscillating control surface downstream of a shock is a prime example. The measured data of Tijdeman and Bergh[12] for two-dimensional flow over a wing with an oscillating control surface is an excellent source for gaining

insight to the problem. One of the major results given was the time history of the upstream shock during the control surface oscillation. In one particular case, M_∞ =0.90, the shock movement was shown to cover as much as 12% to 15% of the wing chord for a control surface motion of only 1.5 degrees. The interesting point was that for the 6% thick airfoil section used, the control surface amplitude appeared to be about the same as the boundary layer thickness. Since the oscillatory pressure amplitude forward of the shock was very small, the shock motion was primarily due to downstream disturbances only. In other cases, the variation of shock strength with motion was also evident. For M_∞ =0.875, it was shown that the shock wave vanished at its forwardmost position for a control surface amplitude of $\pm$3 degrees. What is important in this discussion is the fact that such small pressure fluctuations can create large shock movements as well as substantial variations in strength.

Another item that deserves some attention is the effect of viscosity and flow separation. In steady or quasi-steady flow, separation effects are not well understood quantitatively, but they can be readily observed in experimental studies. In unsteady flow, however, the simple low frequency mechanism is complicated by the fact that separation is itself an unsteady

phenomena. A means of determining unsteady separation effects has been given by Ericsson and Reding[13] for airfoils oscillating in stalled or nearly stalled flow. The principal inovation is the inclusion of the effect of leeward side acceleration on a pitching or plunging airfoil. This acceleration tends to cancel or diminish the adverse pressure gradient effect and thereby causes an increase in the maximum attainable value of C_L. The method is based on quasi-steady flow. However, in the numerical results presented, reduced frequencies range as high as 0.3 based on semi-chord (two-dimensional flow). Whether or not Ericsson and Reding's method could be useful in unsteady transonic flow cannot be predicted at this time since the approach is oriented towards oscillations about high mean angles of attack in low subsonic flow. The insight provided by the paper could lead to a better understanding of the transonic shock induced separation phenomena as well as establish a basis for developing a method to predict the unsteady effects based on steady flow measurements.

In summarizing the unsteady or high frequency characteristics, a clear cut picture is not possible to define as was done for the steady or low frequency characteristics. A complicating factor is the large shock displacement that apparently occurs with small pressure fluctuations. This

effect tends to spread the shock peak in such a manner as to make it difficult to separate the shock oscillation induced loads with the fluctuating pressure field. It does appear, however, that the effect of lag between the trailing edge and the shock can be observed and predicted at least qualitatively. The effect of unsteady separation is an additional burden which clouds the issue. Some attempts will be made to include separation effects in the numerical applications which, although the model is highly simplified, do tend to improve the solution characteristics.

In the following section, a discussion will be given for the method developed in this research task. No attempt has been made to incorporate special functions to account for shock oscillation induced loads other than the regular lifting surface theory functions already employed. The purpose of the investigation is to determine how well the use of mixed linear theory solutions predicts the characteristics discussed in this section and the best means of application for general problems.

METHOD OF SOLUTION - THE TRANSONIC ALGORITHM

The prediction method investigated in this research is based on the use of general aerodynamic lifting surface (GALS) elements as a means for determining unsteady aerodynamic loadings on lifting surfaces oscillating in mixed transonic flows. The concept as derived originally[9] has been only slightly modified and the basic requirement of a steady mean flow solution as a starting point has been maintained. The method uses subsonic or supersonic lifting surface elements to describe a lifting surface over which the flow is mixed. The principal modification is the addition of a capability which permits the velocity variations in the subsonic or supersonic elements to be partially accounted for. This capability has resulted in improved solutions which point the way towards further refinements in the method.

The linear theory methods for treating subsonic and supersonic flow are discussed in Appendix A and Appendix B, respectively. In modifying the basic methods for use in the transonic method, some investigation was necessary to insure that they were working properly. Several important results were obtained for both subsonic and supersonic linear theory.

In subsonic flow, it was found that different types of lifting surface elements gave slightly different solution characteristics for the same problem. In this case it was suspected that the new type of element converges more rapidly for highly swept wings than does the conventional element. More exhaustive convergence studies are required to settle this matter. For the purpose of the transonic investigation, the results were felt to be completely satisfactory.

In supersonic flow, a special weighting function was developed for the pressure distributions and tried in a limited number of cases. The function was derived from conical flow theory, hence, it contained many of the discontinuities that are encountered in pressure distributions on wings in supersonic flow. Use of this weighting function requires far fewer pressure functions to converge since it is no longer necessary to use smooth functions to construct supersonic discontinuities.

Another important result in supersonic flow was the discovery of the non-integrable singularity in the non-planar supersonic kernel function along the Mach hyperbola (see Appendix D). A means was obtained but not programed for evaluating the finite part of the improper integral by the use of Leibnetz's rule. This was necessary since in the derivation of the kernel function, the consequences were not considered

for interchanging integration and differentiation in supersonic flow. The oversight was natural, however, since the problem does not occur in subsonic flow or in supersonic flow over coplanar surfaces. This problem did not interfer with the transonic study since only coplanar surfaces were considered.

The algorithm for linking subsonic and supersonic linear theory solutions together as a means for treating unsteady mixed transonic flow problems is based on the following two assumptions:

1. The appropriate Mach number for computing downwash at a point is the Mach number of that point.
2. The reduced frequency, $k_\infty = \frac{\omega b_{REF}}{U_\infty}$, is modified according to the local velocity such that ω is held constant. This is approximated as

$$k_l = k_\infty \left(\frac{U_\infty}{U_l}\right) \approx k_\infty \left(\frac{M_\infty}{M_l}\right)$$

The first assumption is justified by the fact that, for any given pressure distribution, the integrated kernel function-pressure function product rapidly becomes independent of Mach number as distance increases either upstream or downstream from a loaded region. The second assumption is mandatory since the physical frequency, ω, must be held constant. The use of the Mach number ratio rather than velocity ratio will

result in a small overestimate (typically about 3% to 4%) of the effect of velocity change. However, as results will show in the next section, such a discrepancy is minor.

With the two basic assumptions, the computational algorithm becomes a simple problem of testing the Mach number of the surface for which downwash is being computed. If the downwash surface is supersonic, then the self-induced downwash as well as all interference effects on that surface are computed with the supersonic kernel function regardless of the interfering surface's Mach number. Likewise, if the downwash surface is subsonic, the subsonic kernel function at that Mach number is used. The value of k in the kernel function is also determined by the local Mach number since the downwash surface sees the same value of ω regardless of what surface the disturbance is emitted from.

A partial accounting for Mach number variations within the subsonic or supersonic elements can be derived from the non-dimensionalization of the downwash-pressure function integral equation. Considering parallel surfaces for simplicity, the downwash at a point (x,y) due to a small loaded region, A_n, may be expressed in supersonic flow as

$$w_n(x,y) = -\frac{\Delta C_{p_n} U_n}{8\pi} \frac{\partial}{\partial z} \iint_{A_n} \frac{z(x-\xi)D(x-\xi-Br)}{r^2\sqrt{(x-\xi)^2 - B^2r^2}} \, d\xi \, d\eta$$

where ΔC_{p_n} is the constant lift amplitude acting over region A_n and U_n is the local steady velocity. To be more general, let H_n be defined as

$$H_n = \frac{\partial}{\partial z} \iint_{A_n} \frac{z(x-\xi)\ D\ (x-\xi-Br)}{r^2 \sqrt{(x-\xi)^2 - B^2 r^2}}\ d\xi\ d\eta$$

or its subsonic counterpart, then for either case

$$w_n(x,y) = -\frac{\Delta C_{p_n}\ U_n}{8\pi}\ H_n \tag{1}$$

Since the function H_n now contains the Mach number characteristics, by virtue of the first basic assumption, this effect may now be ignored for interference since it will always be defined by the local Mach number at the downwash point. Now, it is desired to non-dimensionalize $w_n(x,y)$ with the velocity U_{xy} at the downwash point and ΔC_{p_n} with free stream dynamic pressure q_∞ . Thus, since $w_n(x,y)$ will be summed with other velocity components and then equated to the surface induced downwash, $w_k(x,y)$ where

$$w_k(x,y) = -U_{xy}\ \left(\frac{\partial \tilde{z}}{\partial \tilde{x}} + ik_{xy}\ \tilde{z}\right) \tag{2}$$

we may write

$$\frac{w_n(x,y)}{U_{xy}} = -\frac{\Delta C_{p_n}}{8\pi}\left(\frac{U_n}{U_{xy}}\right) H_n$$

Since it was also desired to non-dimensionalize ΔC_p with q_∞ rather than q_n, we also have

$$\frac{w_n(x,y)}{U_{xy}} = -\frac{\Delta C_{p_{n_\infty}}}{8\pi}\left(\frac{q_\infty}{q_n}\right)\left(\frac{U_n}{U_{xy}}\right) H_n$$

where

$$\Delta C_{p_{n_\infty}} = \Delta C_{p_n}\left(\frac{q_n}{q_\infty}\right) \tag{3}$$

But for one dimensional flow,

$$\frac{q_\infty}{q_n} = \frac{U_\infty}{U_n}$$

and since we are primarily concerned with near normal shocks, the above becomes approximately valid in our case.

Thus,

$$\frac{w_n(x,y)}{U_{xy}} \approx -\frac{\Delta C_{p_{n_\infty}}}{8\pi}\left(\frac{U_\infty}{U_{xy}}\right) H_n$$

or

$$\left(\frac{U_{xy}}{U_\infty}\right)\frac{w_n(x,y)}{U_{xy}} \approx -\frac{\Delta C_{p_{n_\infty}}}{8\pi} H_n$$

Now, the input unsteady boundary conditions

$$\frac{w_k(x,y)}{U_{xy}} = -\left(\frac{\partial \tilde{z}}{\partial \tilde{x}} + i\, k_{xy}\, \tilde{z}\right)$$

are multiplied by the velocity ratio $\left(\frac{U_{xy}}{U_\infty}\right)$ in the integral equation. In the program, the value of k_{xy} is defined as

$$k_{xy} \equiv \frac{M_\infty}{M_{IS}} k_\infty = k_{IS} \tag{4}$$

where M_{IS} is the uniform Mach number assigned to the surface which contains the downwash point rather than the local value at the downwash point (x,y).

As a result of the above discussion, the integral equation that is actually solved by the transonic algorithm is

$$-\left(\frac{\partial \tilde{z}}{\partial \tilde{x}} + ik_{IS}\tilde{z}\right)\frac{M_{xy}}{M_\infty} = \frac{1}{8\pi}\iint \Delta C_{p_\infty}(\xi,\eta)\cdot$$

$$K(x-\xi,\ y-\eta,\ z-\zeta,\ k_{IS},\ M_{IS})\ d\xi\ d\eta \qquad (5)$$

where $\Delta C_{p_\infty}(\xi,\eta)$ is the pressure difference at (ξ,η) divided by q_∞. To be more exact, later versions of the algorithm should permit M_{xy} and k_{xy} to be used in computing the kernel function, thereby permitting the kernel function to change at each downwash point. In this manner, it may be possible to better account for leading edge regions where the flow is continuously accelerated from subsonic to supersonic flow.

Shown in Figure 5 is a flow diagram of the current transonic flow algorithm. The key ingredient is the common set of surface types and pressure function types for both subsonic and supersonic flow as shown in Figure 6. (An exception is the case for steady supersonic flow where a special "supersonic weighting function" has been installed in the computer program for investigating potential payoff.

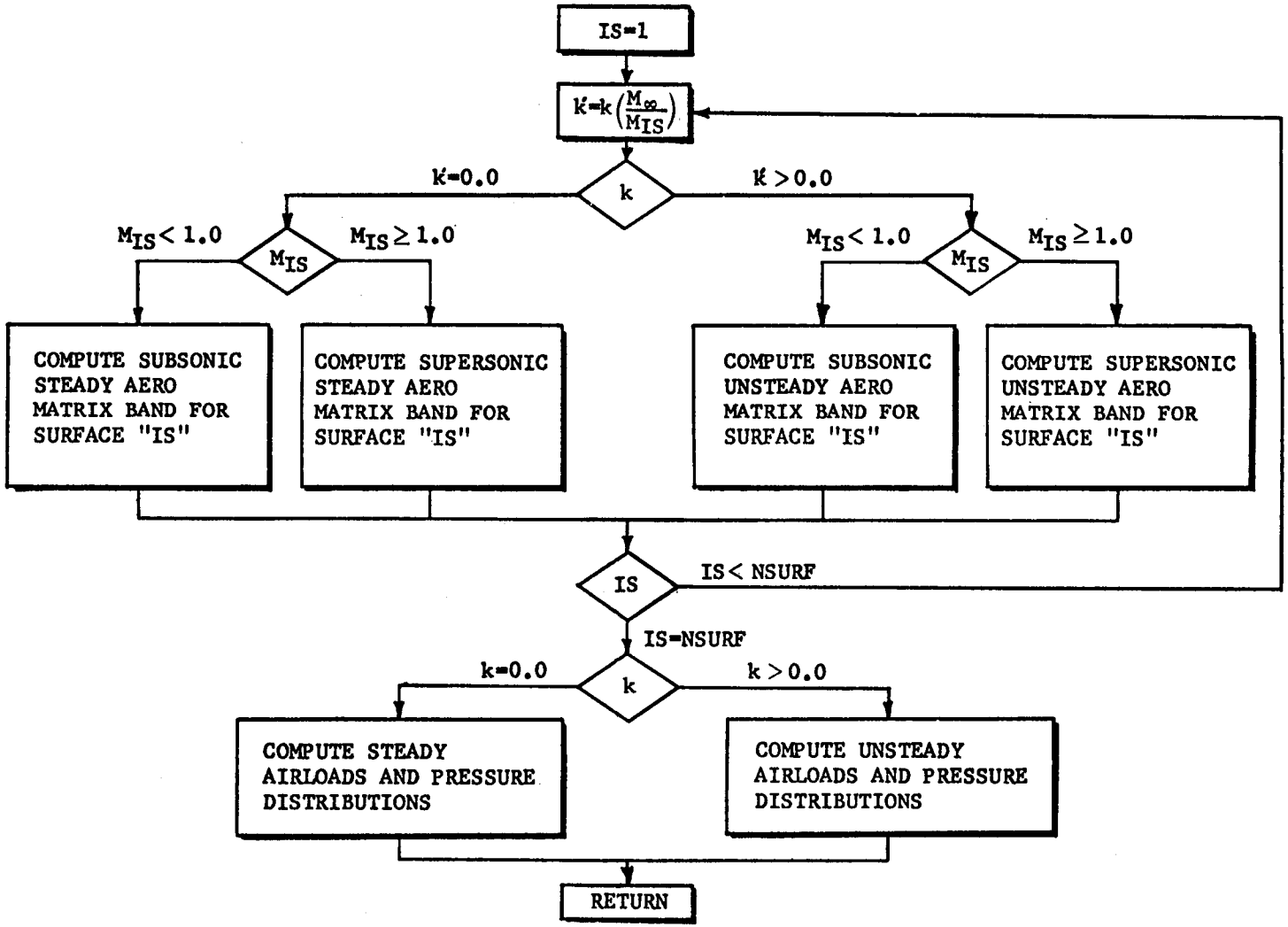

Figure 5 FLOW DIAGRAM FOR COMPUTING MIXED TRANSONIC FLOW LOADS

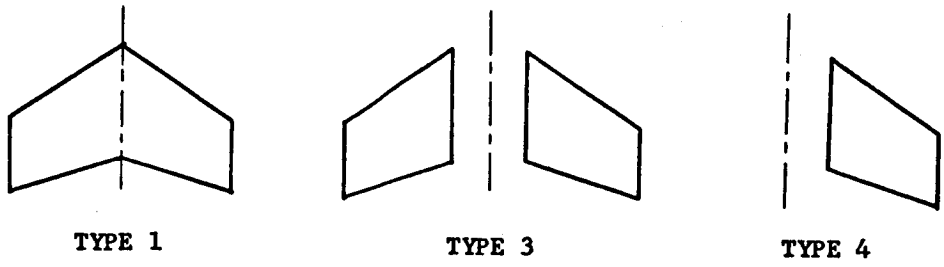

SURFACE TYPES

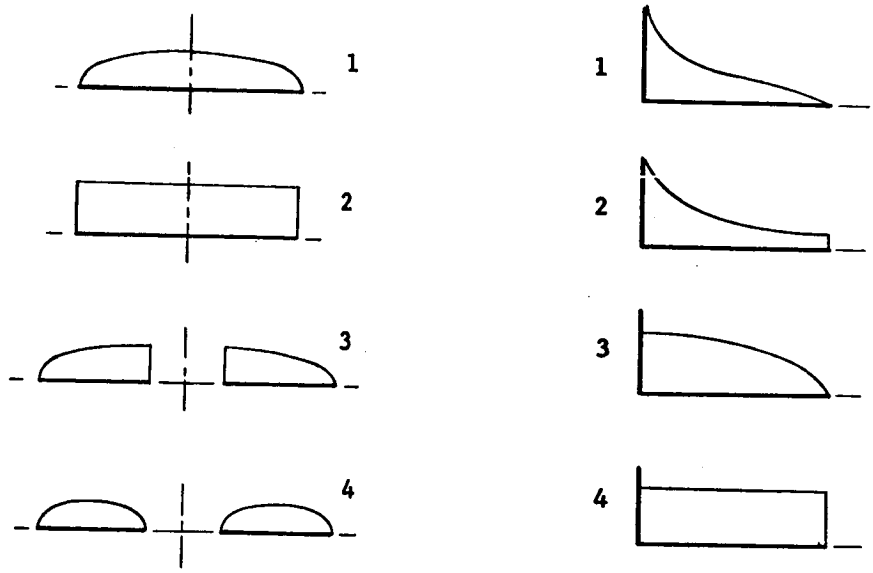

SPANWISE LOADINGS

CHORDWISE LOADINGS

Figure 6 SURFACE AND LOADING TYPES FOR THE GENERAL AERODYNAMIC LIFTING SURFACE ELEMENT

This aspect is discussed in Appendix B.) The integration schemes are also compatible with two exceptions. The difference in the chordwise integration is that in supersonic flow, the limits are from Mach cone to leading edge whereas in subsonic flow they are from trailing edge to leading edge. In the spanwise integration, both techniques are identical with the exception that the supersonic limits are defined by the Mach cone-leading edge intercepts rather than wing tips.

In the next section, the transonic method is applied to a variety of planforms oscillating in mixed transonic flow. The method is consistently shown to yield improved pressure distributions as compared with uniform flow solutions.

APPLICATION OF THE TRANSONIC METHOD

The prediction method described in the previous section was applied to a wide variety of wing configurations in mixed transonic flow. The configurations were both retangular and swept trapezoidal with pitching, bending and control surface motions. The frequency variation ranged from near steady flow to moderately unsteady. In all cases, it was possible to show from moderate to drastic improvement with the transonic method over conventional uniform flow linear theory solutions.

In the following discussions, the first case considered will be a rectangular wing oscillating in a bending mode. For this case, several means for applying the method will be discussed to illustrate some of the areas that have been investigated. The remaining problems simply reflect what was learned in the first case as to how the method should be applied.

Rectangular Wing of Aspect Ratio 3.0 Oscillating in a Bending Mode

In this case results are presented which were obtained with the initially proposed method for treating mixed transonic flow problems. The approach simply proposed to break the wing up into its subsonic and supersonic regions and treat each region according to its assigned Mach number. With the proper

linear theory method, interference was calculated for each surface. The Mach number assigned to the downwash surface determined whether the subsonic or supersonic kernel function was used.

In Figure 7, experimental and theoretical results are shown at midspan for the TND-344[10] case of $\alpha=0^{o}$, $M_{\infty}=0.90$ and $k_{\infty}=0.13$ (based on semi-chord). The dashed line is the uniform flow linear theory solution obtained from the program under development. The solid line is the transonic solution assuming that the forward surface is uniformly supersonic at $M_{l}=1.10$ and extends from the leading edge to 70% chord. The trailing subsonic region is at a $M_{l}=0.90$ and extends from 70% chord to the trailing edge. The reduced frequency, $k_{\infty}=0.13$, is adjusted in each region according to its Mach number. The peaking characteristic is obtained, however, the 180^{o} phase shift is not. Also, the dip in the supersonic pressures near the shock is not correct and is caused by the tip Mach line in the supersonic portion that does not actually exist in the true transonic flow. A three region solution was attempted as a means of removing the tip Mach line effect by allowing the forward 30% of the wing to be at $M_{l}=0.90$. This gave lift which was too high and hence washed out the supersonic portion and drove it negative in both the real and imaginary parts. The

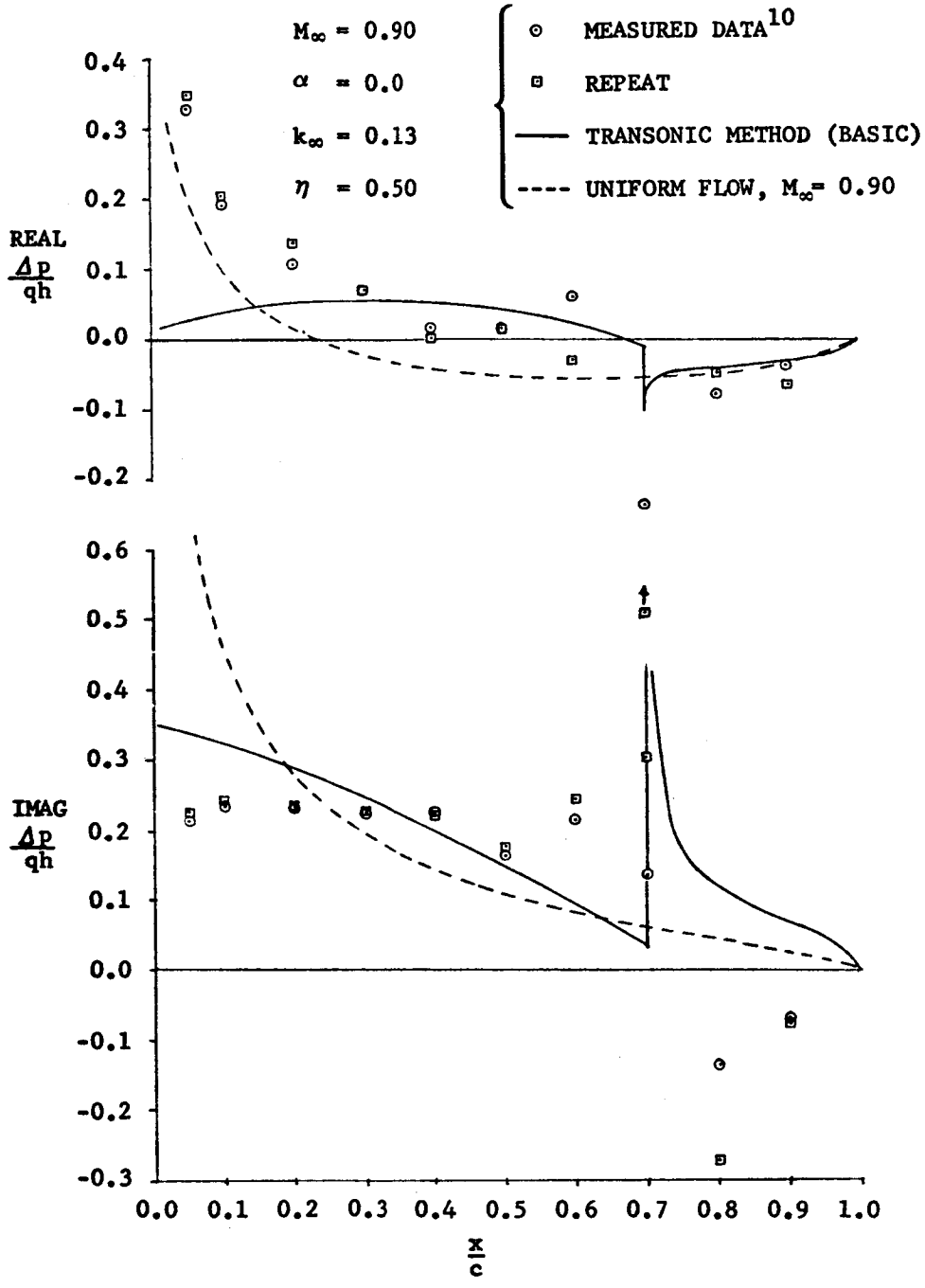

Figure 7 COMPARISON OF UNIFORM FLOW AND THE BASIC TRANSONIC METHOD RESULTS WITH EXPERIMENT

subsonic portion aft of the shock remained unchanged in the solution. As a result, the three region approach was rejected. An alternative will be given in the final recommendations which is felt to be superior.

In Figure 8, some variations of the basic approach are shown. The solid line is again the originally proposed method. The dashed line is a solution obtained with the basic method in which the subsonic region boundary conditions are multiplied by the local chord fraction covered by the subsonic portion. Since the downwash mode is a pure bending mode, the deflections in the aft region are simply multiplied by 0.3. Since the supersonic region is upstream, it is unaffected. The subsonic region is now showing the proper phase relationship with exception of the 70% chord station. Justification for diminishing the downwash on the subsonic region is that apparently the termination at the leading edge by a shock rather than a free edge cancels the aspect ratio effect that tends to increase the isolated C_{L_α} of the surface.

Also shown in Figure 8 is a second modification in the supersonic region (dash-dot-dash line). In this case, the mode deflections are multiplied by the local Mach number ratio which ranges from 1.0 at the leading edge to 1.25 at the shock. Since the Mach number variation is nearly linear (see Figure 2),

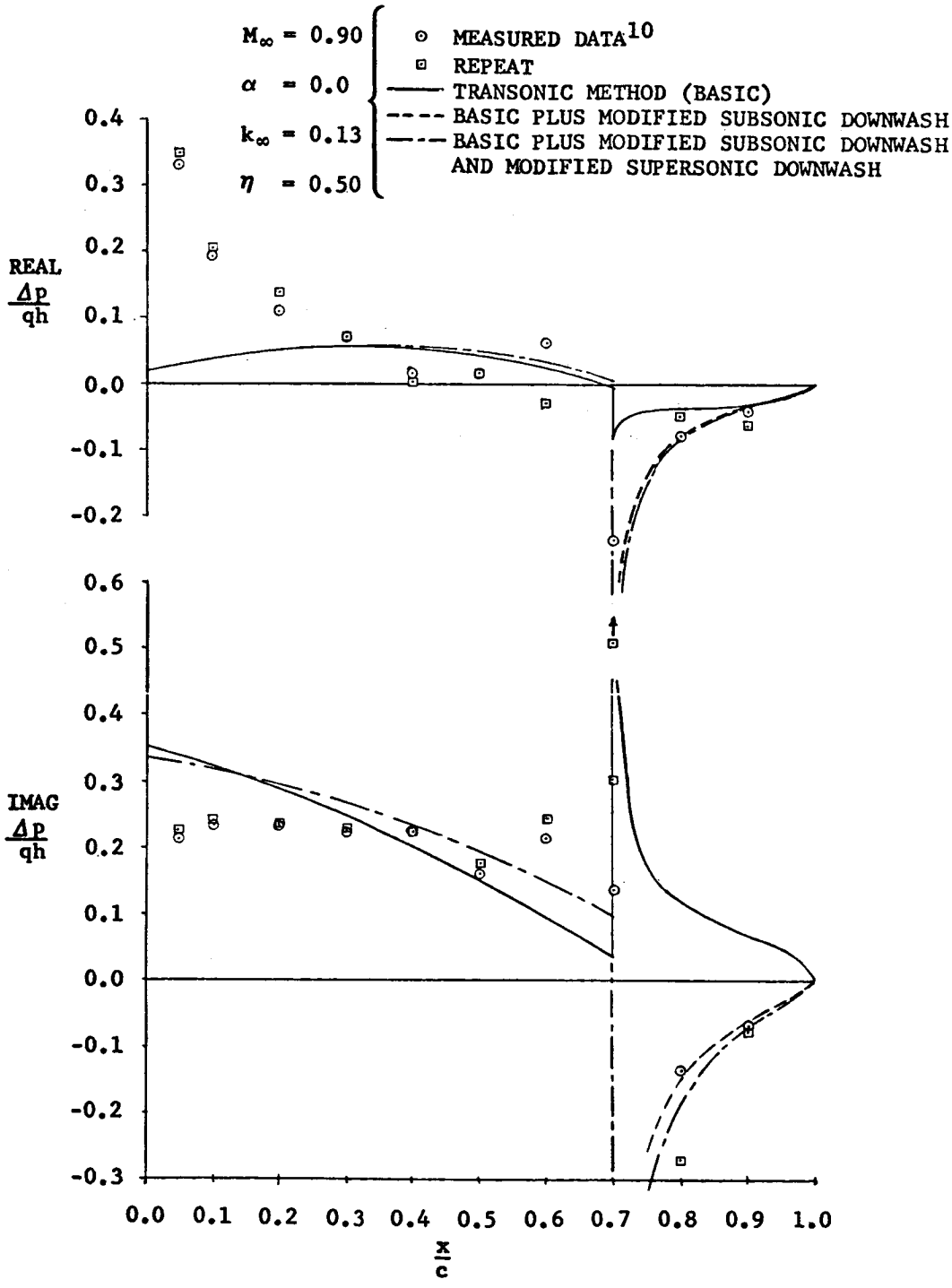

Figure 8 COMPARISON OF THE BASIC TRANSONIC METHOD AND MODIFIED METHOD RESULTS WITH EXPERIMENT

a linear function was used. This modification was made based on an assumption that local perturbations in streamwise velocity are accelerated along with the mean flow. Although this artifice is another semi-empirical correction, it does improve the imaginary part of the solution.

Finally, Figure 9 shows the comparison of the uniform flow solution (dashed line), the transonic solution with the two semi-empirical corrections, and experiment. There is a definite overall improvement with exception of the leading edge region in the real part of the solution. In this case the uniform flow solution is superior. Obviously, a three region solution would help this problem. However, it would destroy many of the other favorable characteristics.

As a result of the experience with the above problem, additional investigation was made into the effect of local mean velocity variations on the basic integral equation of lifting surface theory. Surprisingly enough, the rederivation of the integral equation gave the form in Equation 5 which effectively performs the operation discussed in Figure 8 where the downwash was multiplied by the local Mach number ratio in the supersonic region. Equation 5, of course, requires that the ratio be applied in all regions. It did not provide all that was needed to achieve the 180^{o} phase shift aft of the shock. Results of

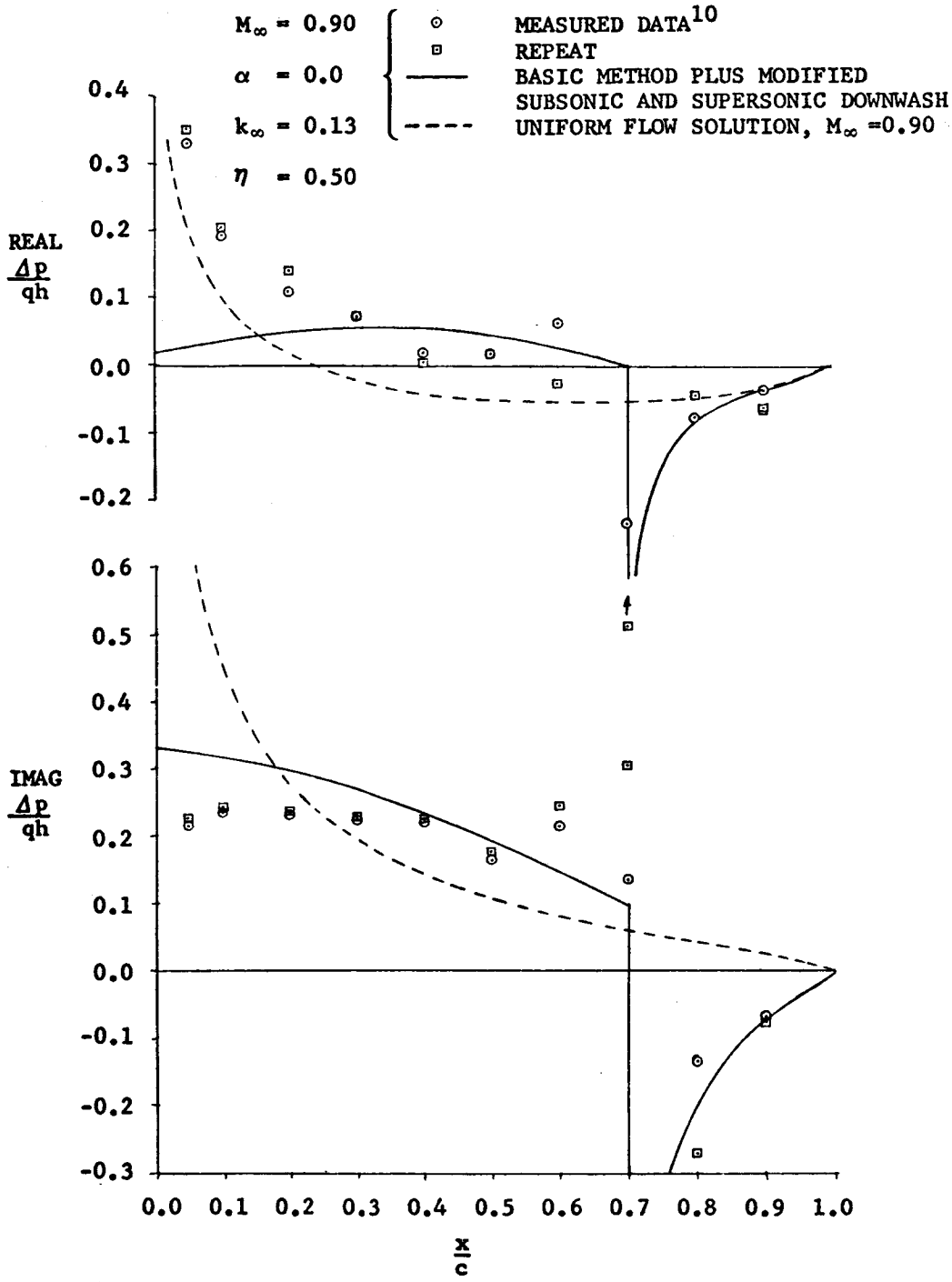

Figure 9 COMPARISON OF THE UNIFORM FLOW AND MODIFIED TRANSONIC METHOD RESULTS WITH EXPERIMENT

application of the final method are shown in Figure 10 where the solid line is the solution obtained by this method and the dashed line is again the uniform linear theory solution. It will be noted that the final version of the transonic method gives results which are better than those shown in Figure 7 for the original method, especially in the vicinity of the shock.

The solution is still not adequate, since the 180^{o} phase shift is not predicted. In order to achieve this, an assumption was made that the flow separated behind the shock and that this effect could be accounted for by multiplying the downwash by 0.5 for all points aft of the shock. Results of this assumption are shown by the short dashed line and, since the supersonic region is not changed, it remains the same. The overall solution is now in excellent agreement with experiment with exception of the real part of the solution near the leading edge. The separation assumption aritifice will be discussed further in the other cases.

	NC	NS
SUPERSONIC REGION	3	6
SUBSONIC REGION	2	6

CONTROL POINT ARRAYS

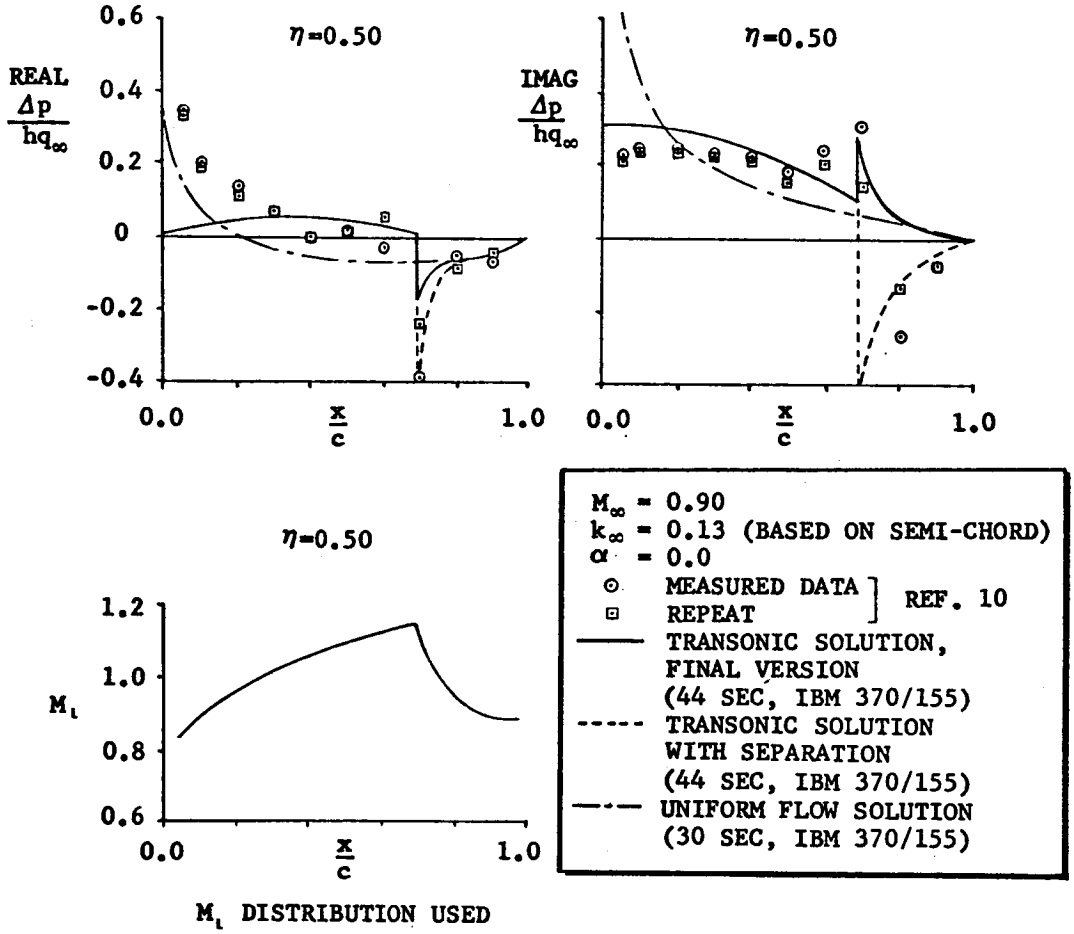

M_t DISTRIBUTION USED

Figure 10 COMPARISON OF UNIFORM FLOW AND THE FINAL TRANSONIC METHOD RESULTS ON A.R. 3.0 WING OSCILLATING IN BENDING

Rectangular Wing of Aspect Ratio 2.0 Oscillating in Pitch

In Figure 11, experimental and theoretical results are shown at 45.4% span on a rectangular wing of aspect ratio 2 oscillating in a unit pitch mode about the 25% chord axis[11]. The flow is mixed transonic with free stream quantities $M_\infty = 0.90$ and $k_\infty = 0.069$ (based on semi-chord). The mean angle of attack is $\alpha = 0$. Although no data was available for the local Mach number distribution, a shock position was assumed based on the unsteady pressure distributions at 60% chord. The distribution of Mach number was taken from Figure 2 which is probably low since the airfoil in this case is an NACA-0008 profile and that for Figure 2 is a 5% thick biconvex profile[10].

The solid line solution is that obtained with the final transonic method and the dashed line is the uniform flow solution. The first point is that the uniform flow solution bears no resemblence to the experimental data except near the trailing edge for the imaginary part. Although the transonic solution shows considerable improvement, particularly forward of the shock, it shows the same disagreement aft of the shock as was noted in the previous problem. Again, application of the separation assumption (1/2 downwash aft of the shock) yields the short dashed line solution which shows much better

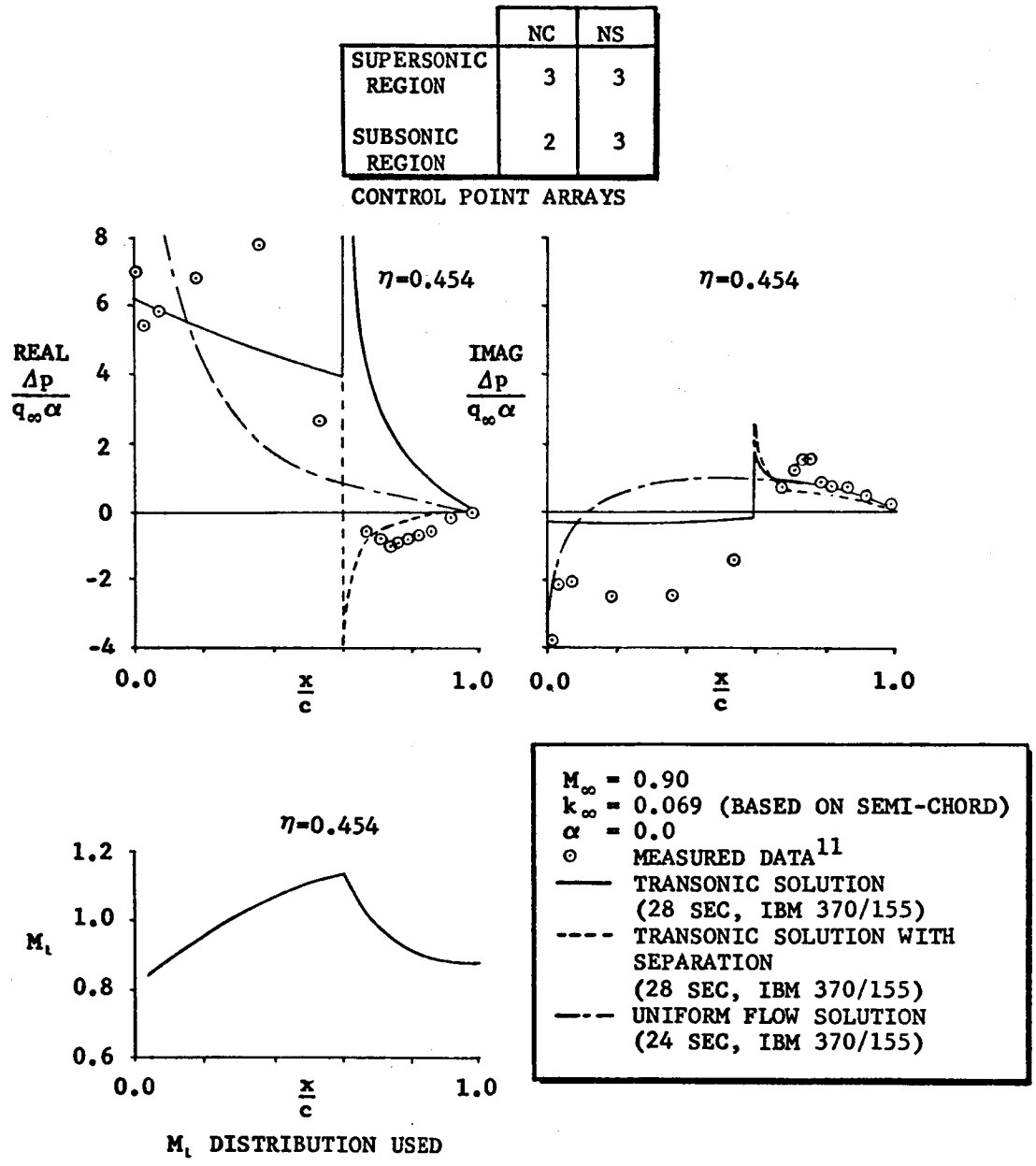

Figure 11 RESULTS FOR AN A.R. 2 RECTANGULAR WING OSCILLATING IN PITCH

agreement with experiment aft of the shock.

The gross under prediction of amplitudes is felt to be due primarily to the experimental data being too high, which was perhaps caused by wall interference. If one scales the real part measured data, say an average of $\Delta p=6.5$ forward of the shock, by the value of $k_\infty = 0.13$ for the rectangular wing in the previous problem, an amplitude of $\Delta p=0.845$ is obtained. Since the wing in the previous problem was oscillating in a bending mode, a further reduction is needed. By comparing theoretical results of the two cases, an average $\Delta p=.25$ can be obtained at midspan if the average value $\Delta p=5.0$ is taken from Figure 11 forward of the shock and multiplied by 0.13 and 0.384. The latter multiplier accounts for differences between the bending mode spanwise displacement distribution and that of the pitch mode (which is constant). (In this exercise, the unsteady effects of $\frac{\partial z}{\partial t}$ are ignored due to the low value of k_∞ .) Multiplying $\Delta p=0.845$ by 0.384 yields $\Delta p=0.325$ which is about 50% higher than that shown in Figure 10 for the imaginary part forward of the shock. If the experimental data in Figure 11 was lowered by about 1/3, the agreement with theory would be more nearly akin to that shown in Figure 10.

The suspicion that wall interference is responsible is based on the fact that the wing chord and span (0.280 meter) were about 1/4 of the wind tunnel test section dimension (1.0 x 1.0 meter^2). The same was true for the model in the previous problem which is known to have wall interference effects. Since the wing in the current problem was thicker and the reduced frequency lower, it is quite probable that the unsteady interference effects were even worse.

Regardless of the source of disagreement, the transonic method does provide a solution which shows much better agreement with experiment. It has also been shown again that the separation assumption artifice further improves the solution.

Swept Trapezoidal Wing With Roll Excitation

In this case, a swept trapezoidal wing studied by Becker[14] was considered which was forced to oscillate in a bending mode by roll excitation at 100 Hz. The bending mode also contained some twist motion. In Figure 12, the planform and the mode shape is shown. The control point array on the planform is that used for the uniform flow solutions. For the non uniform solutions, the downwash point arrays and planform subdivisions are shown in Figure 13.

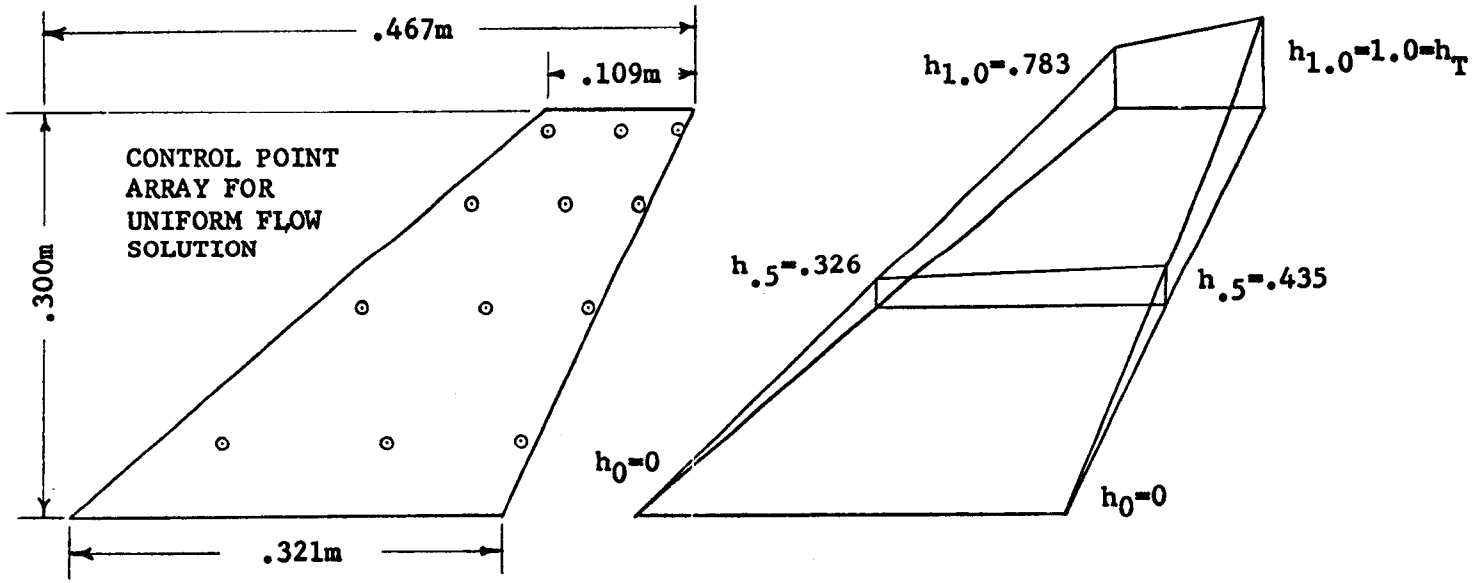

Figure 12 GEOMETRY AND MODE DATA USED FOR THE TRAPEZOIDAL WING OSCILLATING IN BENDING

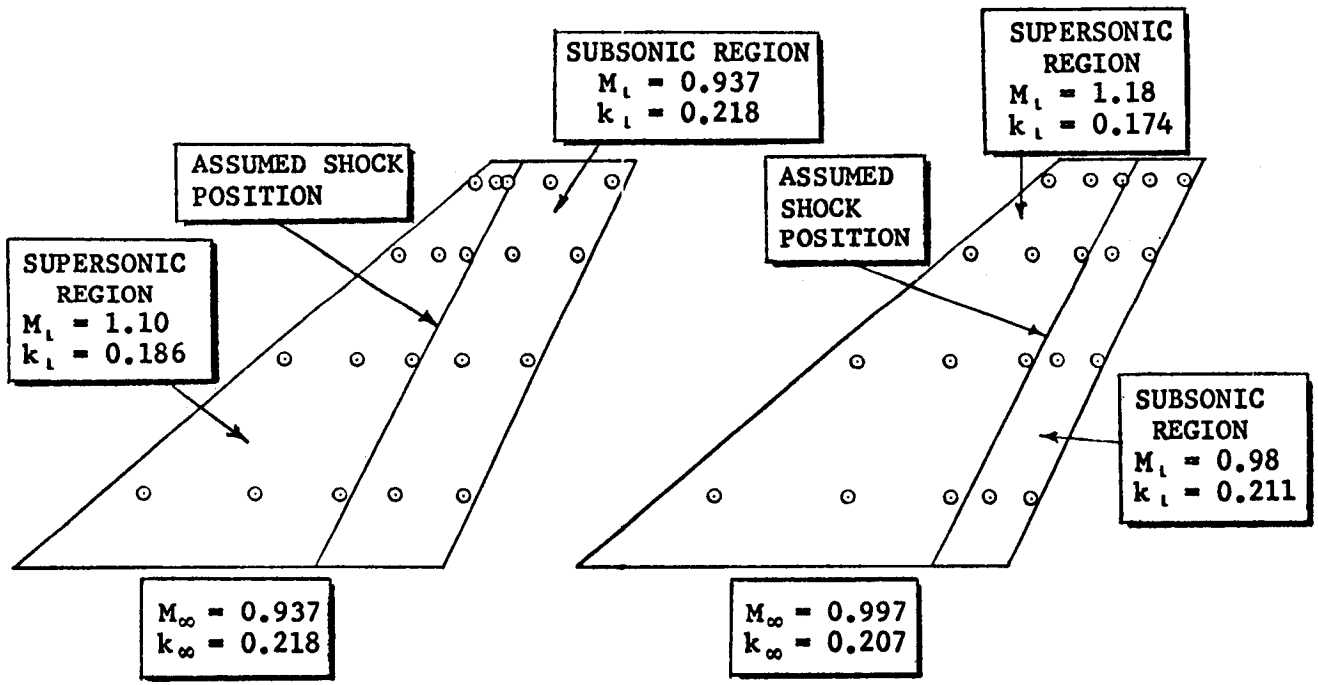

Figure 13 GEOMETRY FOR TRAPEZOIDAL WING TRANSONIC SOLUTIONS, M_∞ =0.937 AND M_∞ =0.997

The first solution considered is subsonic where the present method for uniform flow is compared with experiment and a theoretical solution also given by Becker obtained with Laschka's method. This case is presented as a means of establishing possible sources of disagreement. The flow conditions are M_∞=0.80 and k_∞=0.253 (based on 1/2 MAC). Since the flow is subcritical, it would be expected the theory and experiment should agree fairly well. The data shown in Figure 14 at 55.6% span indicate large discrepancies between both theories as well as between the theories and experiment. The principal cause of the disagreement between theories is attributed to the insufficient data available in the report for determining the mode shape. This is the most likely source of error since it has been shown[15] that the present method and Laschka's method agree very well for wings of this type. Moreover, it seems that Becker had not determined the proper mode shape to use in the theoretical prediction since Laschka's method is far more accurate than Figure 14 indicates. Thus, in considering the following comparisons between theory and experiment in transonic flow, the discrepancy in the mode shape used and that actually occurring in the experiment must be kept in mind.

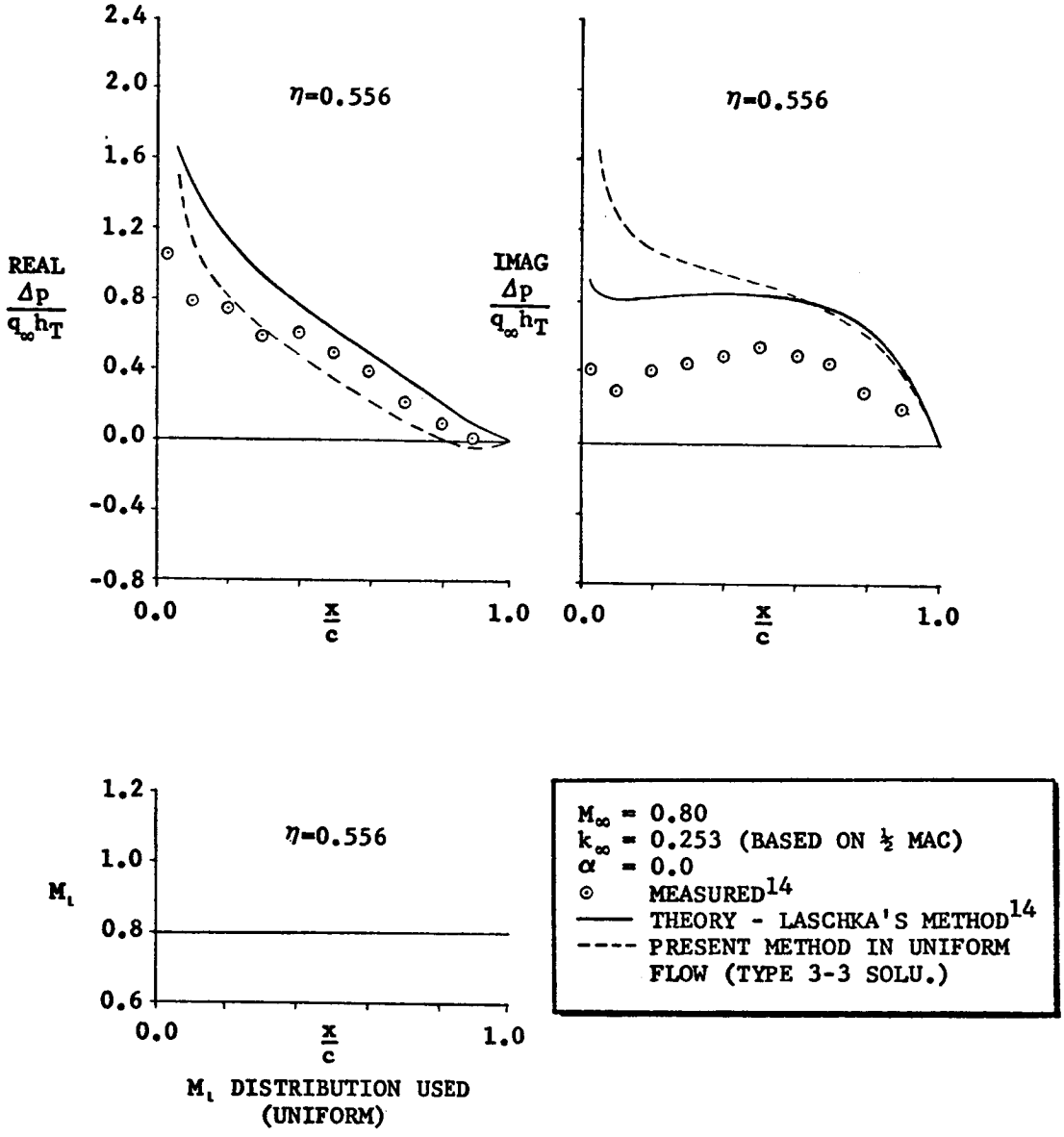

Figure 14 COMPARISON OF THEORY AND EXPERIMENT ON OSCILLATING TRAPEZOIDAL WING IN UNIFORM FLOW

In Figure 15, the chordwise pressure distribution is shown at 55.6% span where the free stream conditions are M_∞ =0.937 and k_∞ =0.218 (based on 1/2 MAC). For this case, the flow is mixed transonic flow for a mean angle of attack, α =0. Symbols are given for both upper and lower surface measurements which show a considerable spread in data. Not all data points were available from the figure in the report due to their being off scale. (Where this is true, a symbol is given with an arrow pointing in the direction that it is suspected to occur.) The dashed line solution is that obtained with the uniform flow theory method. The solid line solution is the transonic solution for which the shock structure was assumed as shown in Figure 13. In comparing the uniform flow and transonic solutions, it is apparent that the transonic method is definitely superior. Considering the disagreement at M_∞ =0.8 in Figure 14, it is even more apparent that if the correct mode shape was known, the agreement between the transonic method and experiment would be excellent. In this case, the separation assumption was not necessary.

In Figure 16, the free stream conditions are changed to M_∞ =0.997 and k_∞ =0.207. The shock is much farther aft and again the transonic solution shows an improvement over uniform flow theory with exception of the imaginary part of the solution

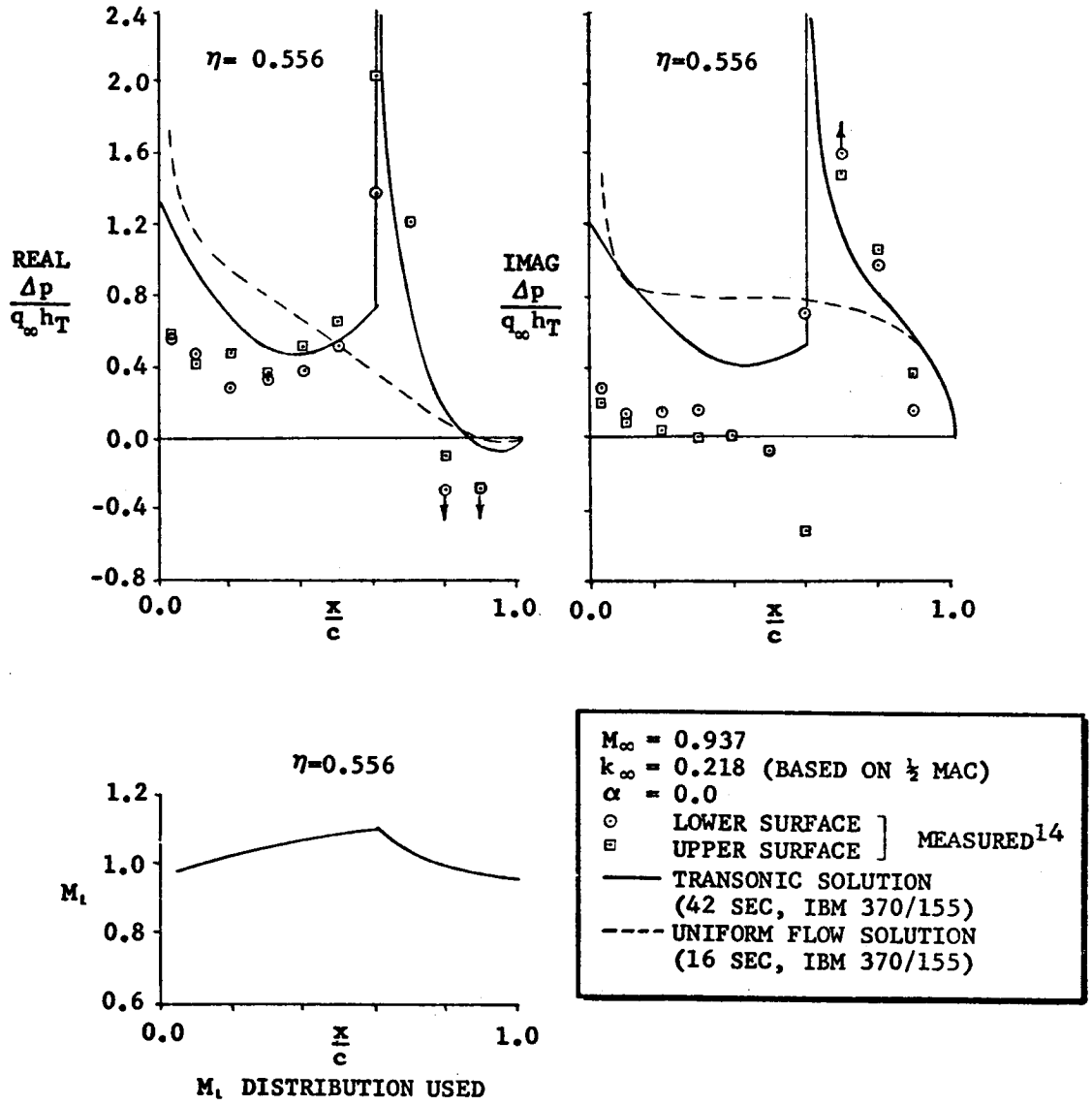

Figure 15 RESULTS FOR AN OSCILLATING TRAPEZOIDAL WING (BENDING) IN MIXED TRANSONIC FLOW, M_∞ =0.937

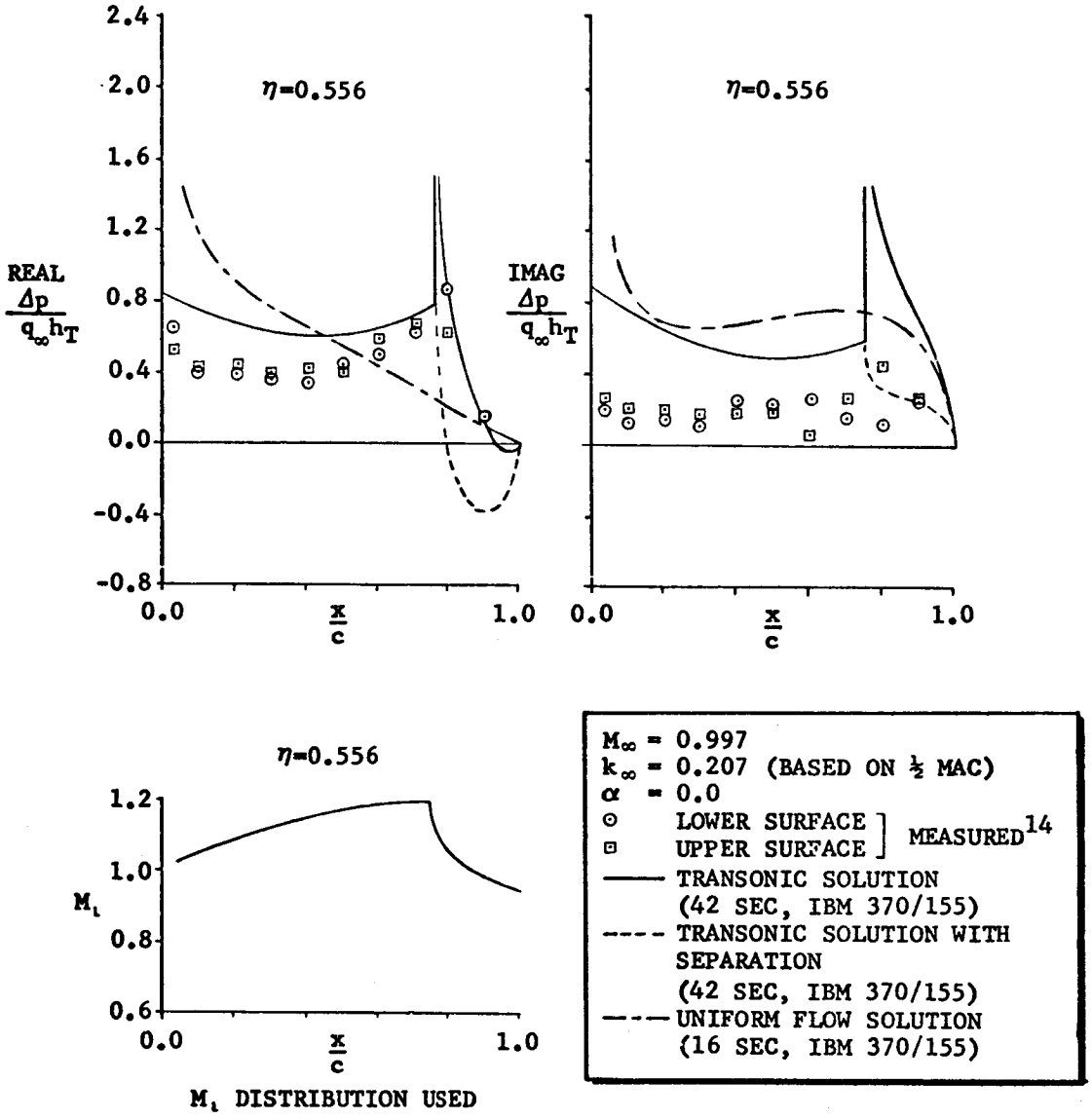

Figure 16 RESULTS FOR AN OSCILLATING TRAPEZOIDAL WING (BENDING) IN MIXED TRANSONIC FLOW, M_∞ =0.997

aft of the shock. In this case, the separation assumption is employed which improves the imaginary part but causes the real part to be under predicted aft of the shock. Without the discrepancy in modal data, it is seen that the transonic solution would probably agree quite well with experiment. By lowering the pressures forward of the shock, the real and imaginary parts would increase and be more in agreement with experiment. The same would be true for the data in Figure 15.

The data obtained in this study are almost certainly affected by wall interference. The model dimensions of a semi-span of 0.3 meters and MAC of 0.215 meters are quite large compared to the test section dimensions of 0.42 x 0.55 meters[2]. Later investigations should include an image system to determine how severely this data might be affected. It is possible that the disagreement just discussed is due more to interference rather than insufficient modal data.

Swept Trapezoidal Wing With an Oscillating Aileron

The final case studied is concerned with a low aspect ratio swept trapezoidal wing with an oscillating inboard aileron in mixed transonic flow. The conditions are M_∞ =0.942 and k_∞ =0.386 (based on 1/2 MAC). Measured data were obtained by Bergh, Tijdeman, and Zwaan[16] which included Mach number maps

over the entire wing as well as oscillatory pressure distributions. The configuration is shown in Figure 17. Comparing the planform dimensions with the test section dimensions of the tunnel used, 2 x 1.6 meters^2, it is apparent that the data should show far less wall interference effects than in the cases previously considered in the current study.

Given in Figure 17 is the GALS element arrangement and downwash point array used to obtain the uniform flow solution. Also shown is the geometry and downwash point array used in the transonic solution. Since only the aileron was oscillating, the wing area was ignored upstream of the tip shock and the Mach line emanating from the aileron apex. The dashed line indicates the tip shock location which cuts across the supersonic element. Because of current restrictions in the computer program the supersonic element could not be broken up accordingly. (The restriction is a result of the program not being completely checked out for non-trapezoidal surfaces in unsteady supersonic flow.) If the subsonic region could be extended into the small triangular space between the hinge line and shock, an improvement in the solution could be obtained as will be pointed out. Only the subsonic portion of the M_t distribution shown in Figure 17 was used in the solution at all span stations on the aileron since the downwash was zero at all points off of the aileron (see Equation 5).

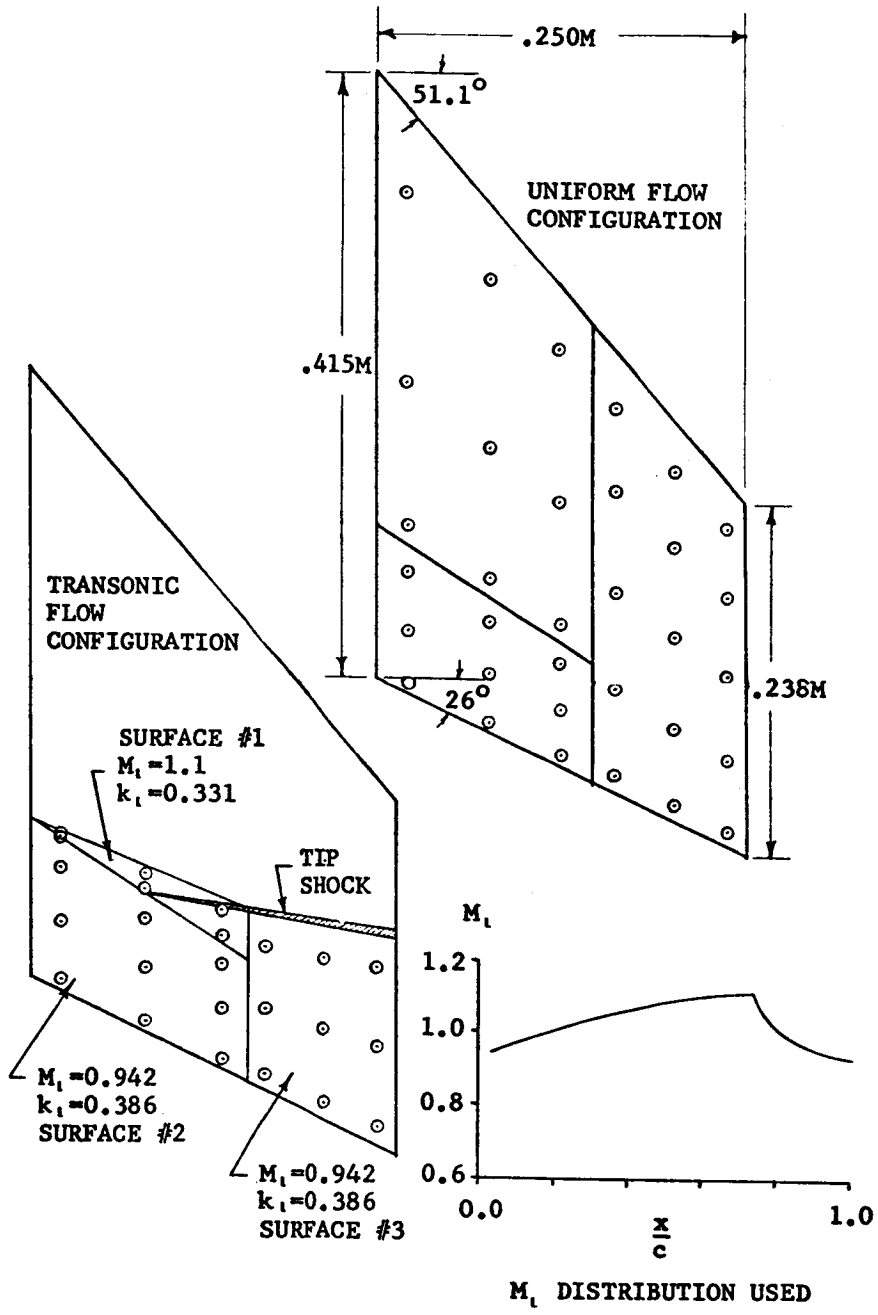

Figure 17 GEOMETRY FOR THE TRAPEZOIDAL WING WITH AN OSCILLATING AILERON IN MIXED TRANSONIC FLOW

The results for the uniform flow and transonic solutions are shown in Figure 18 along with the experimental data. The agreement between uniform flow theory and experiment is very good on the aft 25% of the wing including the aileron. It is not so good, however, on the forward 75%. The transonic solution shows excellent agreement with experiment at all span stations considered. Since the results are concentrated about the tip of the aileron, this case becomes a severe test of the method.

A very interesting point is the prediction of the negative peaks in the imaginary part forward of the hinge line and aft of the shock at outboard stations. This characteristic seems to be common on oscillating control surface problems in transonic flow and was observed repeatedly by Tijdeman and Bergh in two-dimensional flow[12] and in this case for three-dimensional flow. What is more interesting is that the prediction shows the peak to extend outboard of the aileron where the experimental data seems to confirm the fact.

The over prediction of pressures on the aileron seems to be common to both solutions, especially for the real parts. If one assumed that the flow was separating and invoked the separation artifice, all pressure amplitudes would be halved since the only non-zero boundary conditions are on the aileron.

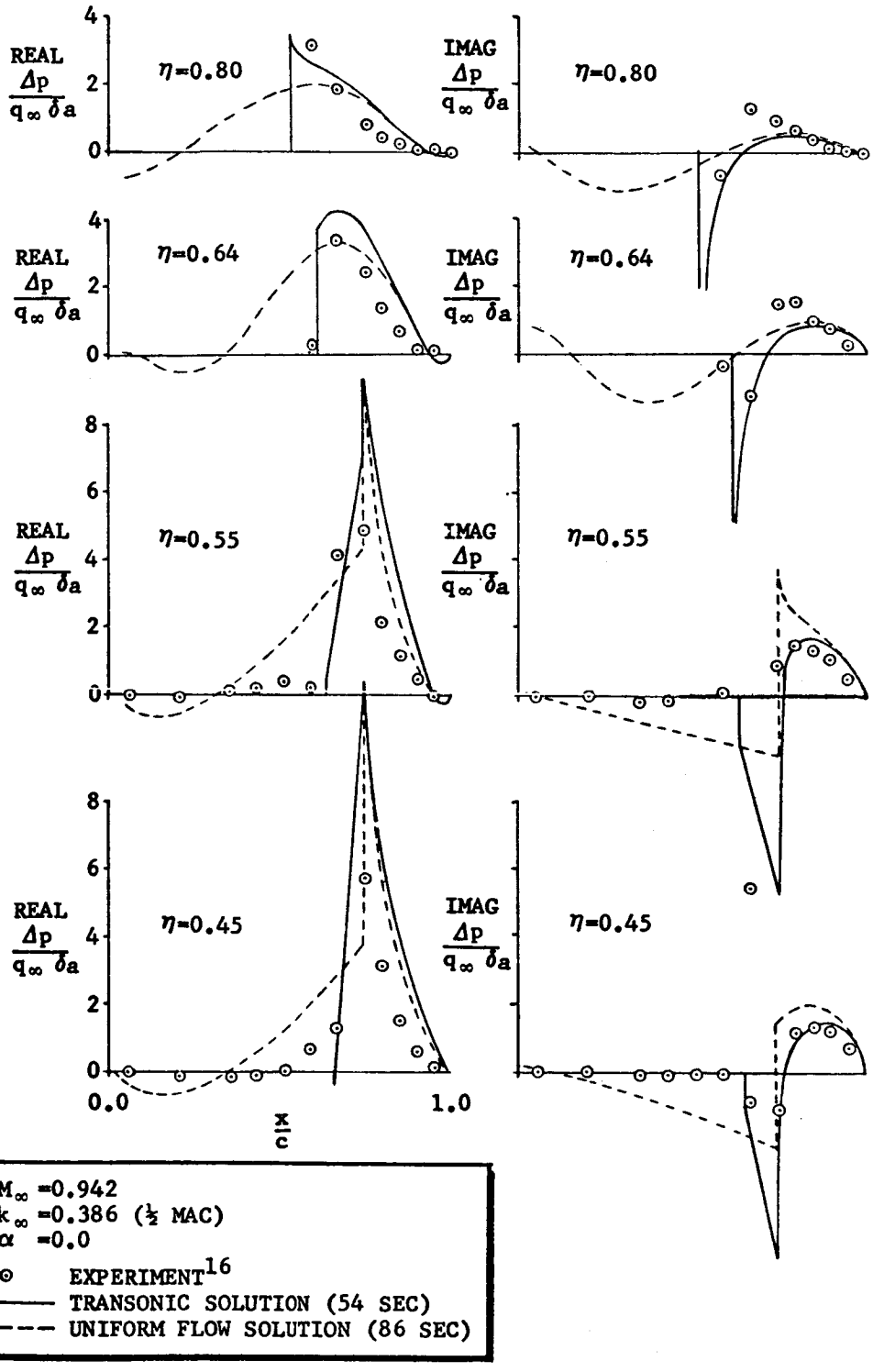

Figure 18 RESULTS FOR A TRAPEZOIDAL WING WITH AN OSCILLATING AILERON IN MIXED TRANSONIC FLOW

This would bring the lift over the aileron more into agreement for the real part. However, the imaginary part would be under-predicted. Also, both parts of the solution outboard of the aileron would be under predicted. It is possible that only the outboard region of the aileron is separated since the shock does not extend completely to the wing root. If data were available more near the mid span of the aileron a more rational assessment could be made of the problem.

Another characteristic that could be improved is the peak aft of the shock at the η=0.55 span station. If it were possible to set up the small subsonic triangle aft of the shock and forward of the hinge line as was discussed above, a peak aft of the shock would be obtained as well as at the hinge line. This would improve the agreement in shape of the pressure distributions. However, the total integrated value of lift would probably not change significantly.

Unlike the previous examples, the transonic solution in this case was cheaper than the uniform flow solution. This was due to the fewer number of control points required, 24 for the former and 33 for the latter, as a result of ignoring the forward portion of the wing in the transonic solution. In a practical dynamics problem, however, all of the surface would be used since the natural modes would produce loads in the

portion that was ignored. The computer time would increase to about 100 seconds per solution.

This case represents the most difficult problem attempted with the transonic method. Because of the high confidence in the measured data, it is felt to represent a valid yardstick by which the transonic method can be evaluated. The prediction of characteristics is excellent, however, the amplitudes are over predicted in some areas, especially on the aileron. With a better understanding of the problem as reflected by some of the thoughts discussed in the section "Transonic Characteristics - A description of the Problem," it is felt that these discrepancies can be almost eliminated or their effects at least minimized.

DISCUSSION - SEPARATION ASSUMPTION OR SOMETHING ELSE?

In the results presented, it has been possible to obtain solutions with the transonic method that show significant improvement over linear theory solutions for uniform flow. The transonic method appears to work as well as the subsonic and supersonic methods of which it is comprised. One difficulty that was encountered, however, is not related to the combining of supposedly incompatible methods. The assumption of separated flow seemed to be necessary in order to obtain proper results aft of the shock in almost all cases. The cases that did not require the assumption were those in which the shock was more forward (at about 50% chord) and/or the reduced frequency was high. This is a rather curious situation in that these are the conditions in which the lag between the trailing edge signals and the shock position is increased over that occurring where the shock is close to the trailing edge or the frequency is low. A prime example of this effect is the comparison of data in Figures 15 and 16. In the first case, the shock was at about 60% chord and the frequency was $k_\infty = 0.218$. The separation assumption was not needed, particularly in this case since it would have caused further under prediction aft of the shock. In Figure 16, the frequency is about the same,

k_∞ =0.207. However, the shock is farther aft at about 75%. The separation assumption was used to bring the imaginary part into agreement. However, the real part was under predicted somewhat.

Thus, it seems that the separation assumption, which simply halves the downwash amplitude in the separated region, is not completely satisfactory. Two reasons can be postulated:

(1) The separation phenomena is frequency dependent due to the tendency of favorable surface motion induced accelerations to counteract adverse pressure gradients and delay stall. Hence, a phase angle change should be introduced.

(2) The phenomena is not due to separation since at very low frequencies the characteristics should be quasi-steady which yields a 180^o phase shift in lift aft of the shock due to its movement.

The first reason for the difficulty is probably true since, as was pointed out in the section on "Transonic Characteristics ...," separation is in itself an unsteady phenomena and is likely to change characteristics when excited by unsteady flow of the same frequency range. The second reason is also true and probably more important for the cases considered in this study. This point deserves further discussion.

The originally proposed hypothesis for development of the transonic method was based on an abservation that shock oscillation peaks appeared to be similar to leading edge singularities in subsonic flow. This has been shown repeatedly to be approximately true for amplitude but not for phase. Hence, it is felt that an additional function is needed which accounts for the shock behavior since the combined linear theory method for transonic flow does not contain any special relations.

A promising area of investigation is the small disturbance equation of transonic flow as discussed by Murman and Cole[7]. This equation is for a velocity potential ϕ where

$$u = \phi_x \quad \text{and} \quad v = \phi_y$$

and is expressed as

$$\left[K - (\gamma + 1)\, \phi_x \right] \phi_{xx} + \phi_{yy} = 0$$

where

$K = \frac{1-M_\infty^2}{\delta^{2/3}}$ = transonic similarty parameter

δ = thickness to chord ratio of the airfoil section

γ = ratio of specific heats

$\bar{y} = \delta^{1/3} y$

The equation would have to be modified for unsteady flow and perhaps for three-dimensional flow. Since the equation does contain the shock jump conditions as was pointed out in Reference 7, some excellent insight would be provided by

studying its local solutions even in steady two-dimensional flow. Thus, it is anticipated that local functions could be derived similar to those obtained by Landahl[17] for control surface singularities. By extending the local solutions to include the trailing edge, the proper (or at least approximate) lag characteristics could be obtained for unsteady flow.

As to how the shock induced function would be incorporated into the aerodynamic procedure, guidance would be provided by the small disturbance equation. Since the starting point is a solution to the equation for the limit as $\phi_x \rightarrow 0$ both forward and aft of the shock, no real difficulty is anticipated. The treatment of such singularities in the collocation methods will not present any difficulties since the singularity will always be on a surface boundary. This is a direct result of the use of GALS elements to treat the transonic problem.

CONCLUSIONS AND RECOMMENDATIONS

This report has presented the results of a study to determine the feasibility of using combined subsonic and supersonic linear theory as a means for solving unsteady transonic flow problems economically and yet realistically. The method developed was shown to work reasonably well in that it provided solutions which showed improved agreement with experimental data over those obtained with uniform flow theory without any significant increase in cost. Agreement was improved in several cases by the use of a simplified assumption that the flow was separated behind the shock. The occurrence of separation was suspected as not being the true source of disagreement, however, when considering the relationship between wake signal propagation and shock position. An overview of the cases considered also confirmed this suspicion.

As a result of the comparison of theory and experiment, it was felt that further research would be fruitfull in the areas of flow separation and oscillating shock induced loads. The flow separation phenomena should be considered in the same manner as Ericsson and Reding have done. It would not be proposed to predict flow separation but instead predict the effects of unsteady flow on separation which is already known to exist. The study of oscillating shock induced loads would

be related to the determination of quasi-steady and unsteady effects of surface pressure fluctuations and wake signals on shock position. This task would not include prediction of the mean shock position, but instead, prediction of the oscillatory perturbations about a stable mean position. The small perturbation equation for transonic flow would be the main tool employed in this study.

Some important results were also obtained in the area of linear theory for both uniform subsonic and supersonic flow. In subsonic flow, it was found that different types of lifting surface elements gave slightly different solution characteristics for the same problems. In this case it was suspected that the new type of element converges more rapidly for highly swept wings than does the conventional element. More exhaustive convergence studies are required to settle this matter. In supersonic flow, a special weighting function was developed and tried in a limited number of cases. The function was derived from conical flow theory, hence, it contained many of the discontinuities that are encountered in supersonic flow. Use of this weighting function requires far fewer pressure functions to converge in that it is no longer necessary to use smooth functions to construct the supersonic discontinuities. Another important result in supersonic flow was the discovery

of the nonintegrable singularity in the nonplanar supersonic kernel function along the Mach hyperbola. A means was obtained but not programed for evaluating the finite part of the improper integral by the use of Leibnitz's rule. This was necessary since in the derivation of the kernel function, the consequences were not considered for interchanging integration and differentiation in supersonic flow. The oversight was natural, however, since the problem does not occur in subsonic flow or in supersonic flow where all surfaces are coplanar.

In conclusion it is recommended that a unified subsonic, transonic, and supersonic aerodynamic prediction method be developed from the existing program. In order to do so, the following tasks are suggested:

1. Complete debugging operations on the various methods included in the program and add the equations for integrating the nonplanar supersonic kernel function.
2. Extend the unsteady supersonic flow capability to include the supersonic weighting function.
3. Modify the transonic algorithm such that the Mach number at each control point is used to determine whether subsonic or supersonic methods will be used to compute the downwash.

(This means that the regular pressure functions must be used in the supersonic regions for transonic flow, hence, they must be retained in addition to that proposed in 2.).

4. Develop a realistic means for predicting unsteady effects on flow separation.
5. Develop a function which accounts for the effect of unsteady surface pressure fluctuations on shock motion induced loads.
6. Incorporate 4 and 5 into the transonic program.
7. Add on appropriate subroutines to perform computation of generalized forces for flutter and dynamic response analyses. Also, include flutter and mode interpolation packages such that a "one shot" flutter analysis can be performed.
8. Undertake a systematic study to determine sensitivity of pressure distributions and flutter results to variations in the local Mach number distributions and shock geometries.
9. Establish a consistent utilization procedure for routine flutter analysis.

10. Correlate theoretical and experimental flutter results over a wide range of Mach numbers including subsonic, transonic and supersonic values. (A configuration should be chosen for which sufficient pressure data is available to establish the steady mean flow conditions.).

In order to be more efficient, the final program should be capable of computing generalized forces for non-zero or cambered airfoil cases without running two separate problems. The mode shapes should be entered only once, although they would have to be interpolated separately but internally for the upper and lower surfaces. The nonsymmetric case could be treated within a single problem by computing the upper and lower generalized forces separately and then adding them together prior to performing a flutter or dynamic response analysis.

REFERENCES

1. Cunningham, A. M., Jr., "A Collocation Method for Predicting Oscillatory Subsonic Pressure Distributions on Interfering Parallel Lifting Surfaces," AIAA Paper No. 71-329, April 1971.

2. Runyan, H. L. and Woolston, D. S., Method for Calculating the Aerodynamic Loading on an Oscillating Finite Wing in Subsonic and Sonic Flow, NACA Technical Note 3694, August 1956.

3. Rodemich, E. R. and Andrew, L. V., Unsteady Aerodynamics for Advanced Configurations, Part II, A Transonic Box Method for Planar Lifting Surfaces, AFFDL-TDR-64-152, May 1965.

4. Stenton, T. E. and Andrew, L. V., Transonic Unsteady Aerodynamics for Planar Wings with Trailing Edge Control Surfaces, AFFDL-TR-57-180, August 1968.

5. Olsen, J. J., Demonstration of a Transonic Box Method for Unsteady Aerodynamics of Planar Wings, AFFDL-TR-66-121, October 1966.

6. Magnus, R. and Yoshihara, H., "Inviscid Transonic Flow Over Airfoils," AIAA Journal, Vol. 8, No. 12, December 1970, pp. 2157-2162.

7. Murman, E., and Cole, J., "Calculation of Transonic Flows," AIAA Journal, Vol. 9, No. 1, 1971.

8. Bailey, F. R. and Steger, J. L., "Relaxation Techniques for Three-Dimensional Transonic Flow About Wings," AIAA Paper No. 72-189, Presented at the AIAA 10th Aerospace Sciences Meeting, San Diego, California, January 17-19, 1972.

9. Cunningham, A. M., Jr., The General Aerodynamic Lifting Surface Element - An Approach to Solving Unsteady Mixed Transonic Flow Problems, Report No. 064-7-71-4, Convair Aerospace Division of General Dynamics, November 1971.

10. Lessing, H. C., Troutman, J. L. and Meness, G. P., Experimental Determination of the Pressure Distribution on a Rectangular Wing Oscillating in the First Bending Mode for Mach Numbers from 0.24 to 1.30, NASA TN D-344, December 1960.

11. Triebstein, H., Instationäere Druckverteilungsmessungen an einem schwingenden Tragflügel im subsonischen und transsonischen Geschwindigkeitsbereich, Deutsche Luft-und Raumfahrt Forschungsbericht 69-46, July 1969, NASA TT F-13, 337.

12. Tijdeman, H. and Bergh, A., Analysis of Pressure Distributions Measured on a Wing with Oscillating Control Surface in Two-Dimensional High Subsonic and Transonic Flow, National Aerospace Laboratory NLR, The Netherlands, Report NLR-TR-F.253, March 1967.

13. Ericsson, L. E. and Reding, J. P., "Unsteady Airfoil Stall Review and Extension," Journal of Aircraft, Vol. 8, No. 8, August 1971, pp. 609-616.

14. Becker, J., Vergleich gemessener und berechneter instationärer Druckverteilungen für den hohen Unterschall an einem elastischen gepfeilten Flügel, Messerschmitt-Bölkow-Blohm, EWR-Report Nr. 403-69, September 1969.

15. Cunningham, A. M., Jr., "A Rapid and Stable Subsonic Collocation Method for Solving Oscillatory Lifting-Surface Problems by the Use of Quadrature Integration," Materials and Structural Dynamics Volume, AIAA/ASME Eleventh Structures, Structural Dynamics, and Materials Conference, AIAA, New York, 1970, pp. 1-16.

16. Bergh, H., Tidjeman, H. and Zwaan, R. J., "High Subsonic and Transonic Effects on Pressure Distributions Measured for a Swept Wing with Oscillating Control Surfaces," Zeitschrift für Flugwissenschaften, 18 Jahrgang, Heft 9/10, September/October 1970, pp. 339-347.

17. Landahl, M. T., "Pressure Loading Functions for Oscillating Wings with Control Surfaces," AIAA Journal, Vol. 6, No. 2, February 1968, pp. 345-348.

18. Bradley, R. G. and Miller, B. D., "Applications of Finite Element Theory to Airplane Configurations," Journal of Aircraft, Vol. 8, No. 6, June 1971, pp. 400-405.

19. Rodden, W. P., Giesing, J. P. and Kalman, T. P., "New Developments and Applications of the Subsonic Doublet-Lattice Method for Nonplanar Configurations," Paper No. 4, AGARD Symposium for Unsteady Aerodynamics for Aeroelastic Analyses of Interfering Surfaces, Tønsberg Oslofjorden, Norway, November 3-4, 1970, AGARD-CP-80-71.

20. Ii, J. M. and Rowe, W. S., "Unsteady Aerodynamics of Nonplanar Wings and Wing-Tail Configurations of Elastic Flight Vehicles in Supersonic Flight," AIAA Paper No. 72-378, April 1972.

21. Cohen, Doris, Formulas for the Supersonic Loading, Lift and Drag of Flat Swept-Back Wings with Leading Edges Behind the Mach Lines, NACA Report 1050, 1951.

22. Harder, R. L. and Rodden, W. P., "Kernel Function for Nonplanar Oscillating Surfaces in Supersonic Flow," Journal of Aircraft, Vol. 8, No. 8, August 1971, pp. 677-679.

23. Landahl, M. T., "Kernel Function for Non Planar Oscillating Surfaces in a Subsonic Flow," AIAA Journal, Vol. 5, No. 5, May 1967, pp. 1045-1046.

24. Laschka, B. and Schmid, H., "Unsteady Aerodynamic Forces on Coplanar Lifting Surfaces in Subsonic Flow (Wing-Horizontal Tail Interference)," Jahrbuch 1967 der WGLR, pp. 211-222.

APPENDIX A

STEADY AND UNSTEADY SUBSONIC FLOW WITH INTERFERENCE

The subsonic portion of this program has been previously documented in Reference 1 where several comparisons between the present method and other theories and experiment were presented. In this appendix, additional data for the AGARD wing-tail configuration will be given in order to illustrate differences between the new element (Type 3 surfaces, see Figure 6) included in the current program and that reported in Reference 1 (Type 1 surface).

In Figure 19, the lifting pressure distribution is shown for the coplanar AGARD wing-tail configuration in $M_\infty = 0.8$, $k_\infty = 0.0$ flow. The dashed line results are obtained with the Type 3 surface with Type 3 spanwise loadings and the solid line results are obtained with the more conventional Type 1 surface and Type 1 spanwise distributions. The symbols are predicted values from the Woodward method[18]. The three solutions show acceptable agreement on the wing; however, the Woodward solution is consistently high on the tail. Since the present method with a Type 1 - Type 1 solution was shown to agree very well with the Woodward method on a wing tail configuration in Reference 1, it is felt that the small number of elements on the tail in this case is responsible for the over prediction. A comparison of C_{L_α} and C_{m_α} (about wing leading edge apex) is shown for the two solutions with the present method and the doublet lattice[19] and Woodward[18] methods.

	PRESENT THEORY TYPE 1-1	PRESENT THEORY TYPE 3-3	DOUBLET LAT. REFERENCE 19	WOODWARD REFERENCE 18
C_{L_α}	1.258	1.185	1.305	1.325
C_{m_α}	2.333	2.224	-	2.786
Run Time Sec	25	27	-	205
Symbol	——	----		⊙ Wing ⊡ Tail

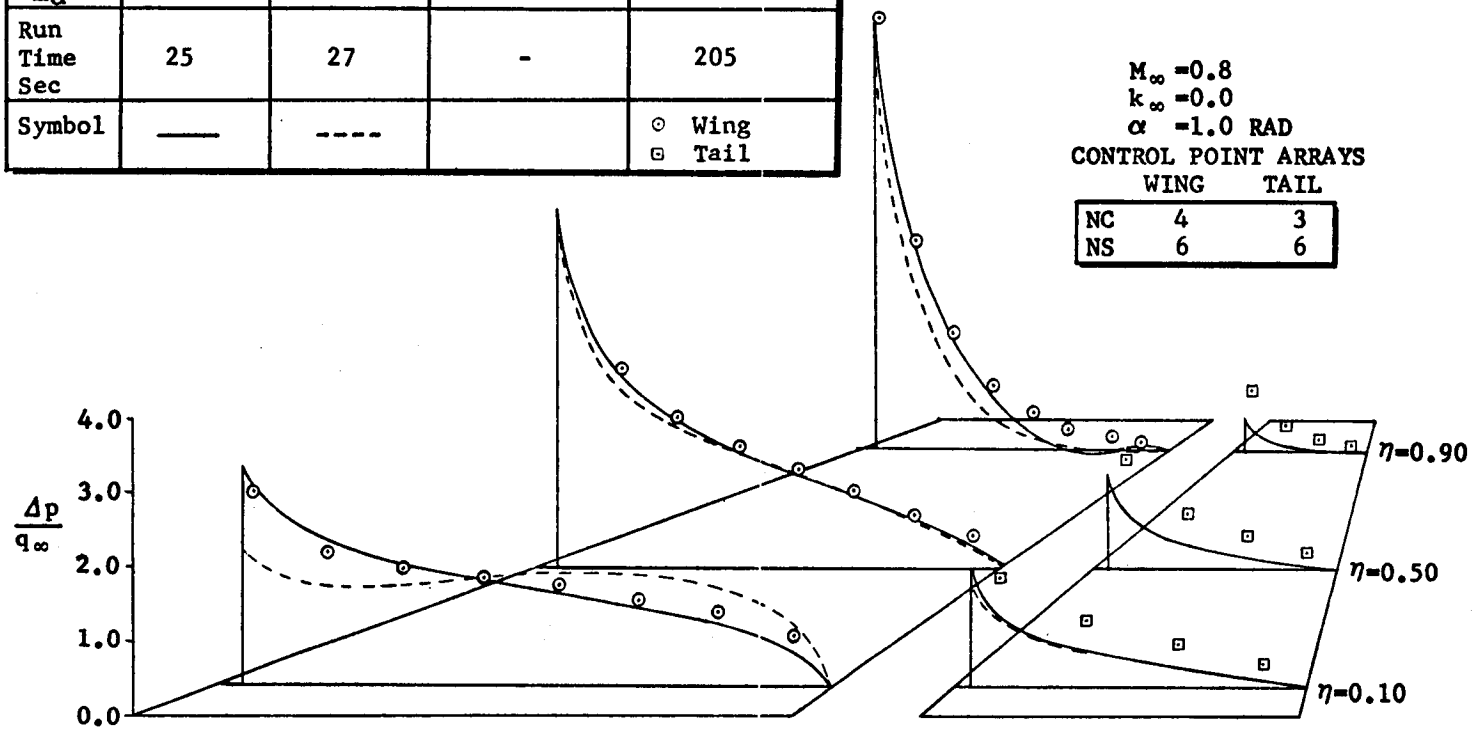

Figure 19 PRESSURE DISTRIBUTIONS AND C_{L_α} - C_{m_α} FOR COPLANAR AGARD WING TAIL CONFIGURATION - SUBSONIC FLOW

The unsteady lifting pressure distribution for the co-planar AGARD wing-tail configuration is shown in Figure 20. The mode is a unit wing-tail plunging motion in uniform flow for M_∞ =0.8 and k_∞ =1.5 (based on semi-span). The distributions shown are again for the Type 1 - Type 1 (solid line) and Type 3 - Type 3 (dashed line) solutions. Results from a convergence study for these solutions are shown in Figure 21 with a comparison with the doublet lattice method. The quantities shown are the real and imaginary parts of the complex lift coefficient divided by (ik). The reference area is the total area (wing + tail) of 2.425 for a wing span of 1.0. Very good agreement is shown for the imaginary part. However, the real part is consistently low. The flaged symbol is the value obtained from the Type 1 - Type 1 solution shown as the solid line distribution in Figure 20. A slight improvement is achieved for the real part which is indicated in both Figures 20 and 21. A perturbation on the Type 3 - Type 3 solution was made with NS=6 where NC=5 on the wing and NC=3 on the tail. This solution is represented by the square symbol and showed practically no change over the base solution with NC=4 on the wing and NC=3 on the tail.

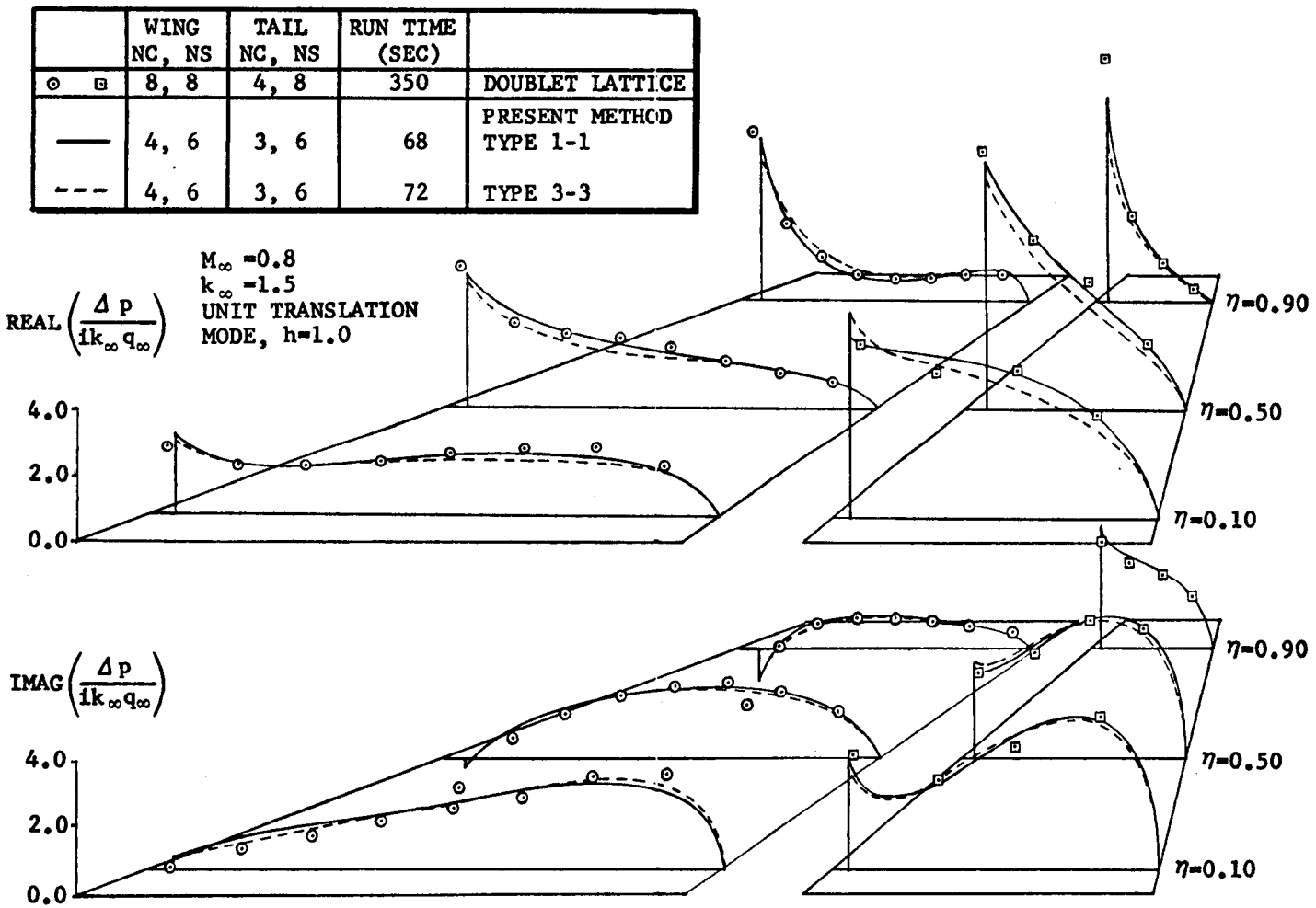

Figure 20 UNSTEADY PRESSURE DISTRIBUTION FOR COPLANAR AGARD WING TAIL CONFIGURATION - SUBSONIC FLOW

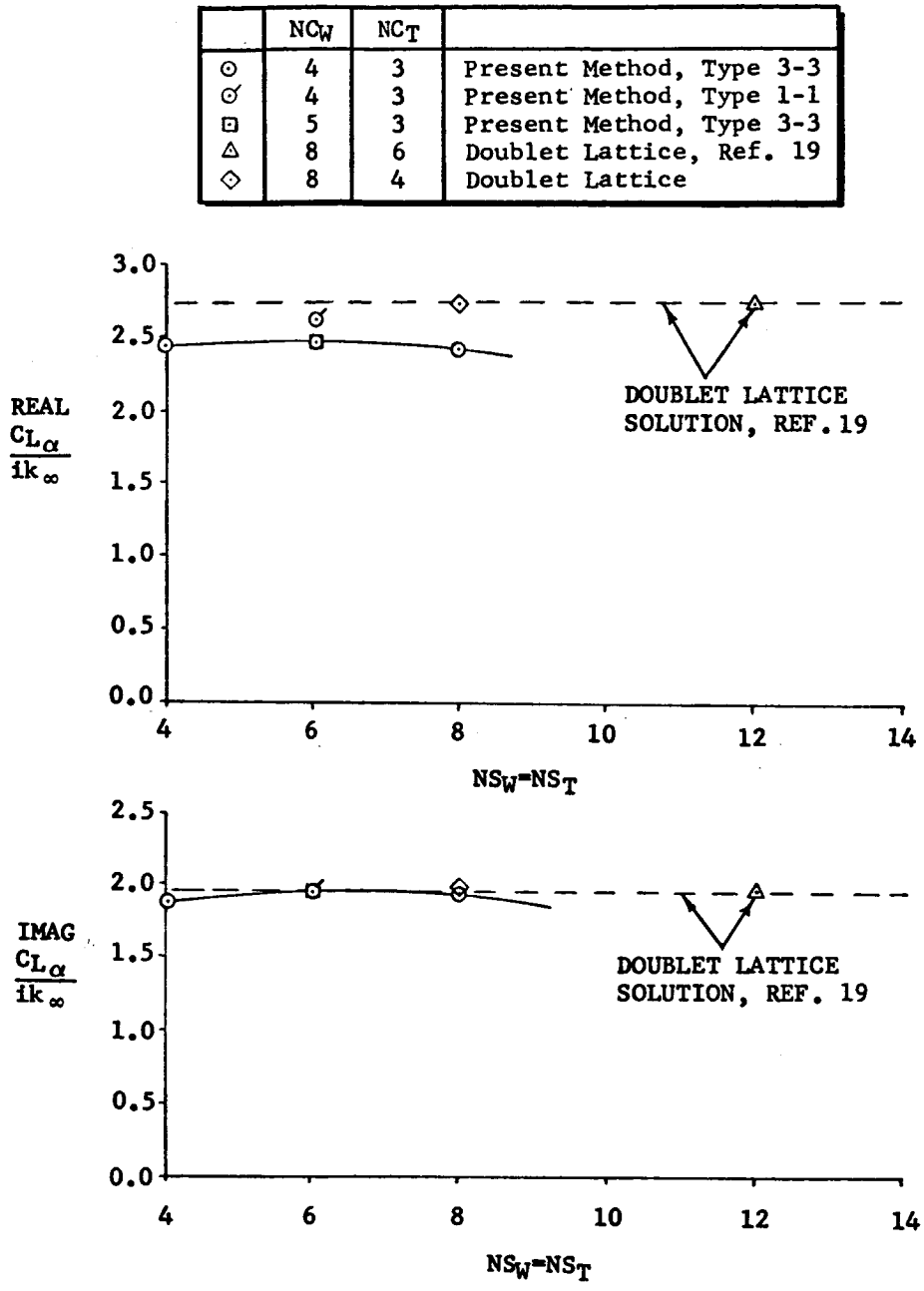

Figure 21 EFFECT OF NUMBER OF SPANWISE POINTS ON C_{L_α} FOR AGARD WING-TAIL IN UNSTEADY FLOW

Although discrepancies exist between the present method and the doublet lattice method, the Type 3 - Type 3 solution permits better treatment of the root region of the highly swept wing. It should logically yield the best solution, thus, it would be desirable to determine which is the best method. In order to accomplish this task, one would have to run extensive convergence studies with the present method. For the purpose of the current study, however, the magnitude of the disagreement was not felt to be great enough to warrant such endeavors since the solutions were close enough to establish the feasibility of the transonic algorithm.

One difficulty that may be the root of the problem is the high value of reduced frequency. For k_∞ =1.5, the wave length is only slightly longer than the configuration. Hence, the differences may be due to differences in evaluating the kernel function. On the other hand, the integration of the kernel function-pressure function product may be the source. Future investigations should include efforts to settle this matter.

APPENDIX B

SUPERSONIC FLOW WITH INTERFERENCE

The supersonic portion of this program is a supersonic extension of the method of Reference 1. The only major change that has been made is in the chordwise integration from the leading edge to the Mach cone boundary. A coordinate transformation is made for each downwash point such that the chordwise variable of integration, $\bar{\xi}'$, varies from -1.0 at the leading edge to +1.0 at the Mach cone. The basic method uses the same surface element and pressure function types employed in the subsonic scheme as shown in Figure 6.

Since the supersonic method was relatively untried in terms of application to real problems, a significant effort was devoted to checking out the algorithm. Based on past experience in steady supersonic flow, it was anticipated that solution convergence would be slow due to difficulties in fitting pressure discontinuities imposed by clipped tips, leading edge discontinuities and interferences with the smooth functions. Thus, a limited investigation was made for steady flow in which a newly developed weighting function for supersonic flow was incorporated. Results of this study will be discussed in the following paragraphs on steady supersonic flow. Under unsteady flow, a brief discussion on a difficulty encountered with the supersonic kernel function will be given along with a comparison between the AFFDL Mach Box Method[20] and the present method for a wing-tail configuration.

Steady Supersonic Flow and the Supersonic Weighting Function

Prior to incorporation of the supersonic weighting function, the steady supersonic method was checked out and used as a basis for developing the unsteady flow subroutine. The subsonic derived pressure functions were used along with the same set of surface types, all of which are shown in Figure 6. Because the supersonic weighting function concept is entirely new, the following discussion will begin with its description and end with a comparison with a solution obtained with the original steady supersonic method. A comparison will also be made with the Woodward method.[18]

The supersonic weighting function is an approximation of the flat plate solutions as obtained from conical flow theory.[23] At present, it is applicable only to simple trapezoidal wings; however, the extension to a general trapezoidal element is certainly feasible.

The basic equation for leading edge and root characteristics is the delta wing distribution. For a subsonic leading edge,

$$m = \frac{\beta}{\tan \Lambda_{LE}} \leq 1.0$$

we have

$$\frac{\Delta p(\bar{a})}{q} = \left(\frac{7.0\ \alpha}{1.75 + \frac{1}{m}}\right) \frac{1}{\beta\sqrt{1-(\frac{\bar{a}}{m})^2}} \qquad \text{(B.1)}$$

where

$$\bar{a} = \frac{\beta(y-y_1)}{x-x_1}\ ,\ x_1,y_1 = \text{Location of leading edge vertex}$$

thus

$$\frac{\bar{a}}{m} = \frac{\left(\frac{y-y_1}{x-x_1}\right)}{\tan \Lambda_{LE}}$$

For a supersonic leading edge, $m > 1.0$,

$$\frac{\Delta p(\bar{a})}{q} = \frac{4m\alpha}{\beta\sqrt{m^2-1}} \left(1 - u(\bar{a})\ P(m) \sqrt{1-\bar{a}^2}\right)$$

where

$$u(\bar{a}) = \begin{bmatrix} 1, & \bar{a} < 1.0 \\ 0, & \bar{a} \geq 1.0 \end{bmatrix}$$

$$P(m) = 1 - \frac{\sqrt{m^2-1}}{4m} \left(\frac{7.0}{1.75 + \frac{1}{m}}\right) \qquad \text{(B.2)}$$

The term $\left(\frac{7.0}{1.75 + \frac{1}{m}}\right)$ which appears in Equations B.1 and B.2 is the approximation used for the exact function

$$\frac{\Delta p_{ROOT}}{q} = \frac{4m\alpha}{\beta E'(m)} \approx \frac{7.0\,\alpha}{\beta(1.75 + \frac{1}{m})}$$

where $E'(m)$ is the complete elliptic integral of the second kind[21] of modulus $\sqrt{1-m^2}$. The fact that the function is not exact presents no problem since the error is multiplicative and is automatically compensated for in the collocation solution.

A tip correction is included for clipped tips. For a subsonic leading edge, $m \leq 1.0$, the lift distribution behind the tip Mach line is constant in the streamwise direction. The amplitude, a function of span only, is given as

$$\frac{\Delta p(\bar{a})}{q} = \left(\frac{7.0\alpha}{1.75 + \frac{1}{m}}\right) \frac{1}{\beta\sqrt{1-(\frac{\bar{a}'}{m})^2}} \left[1-\sqrt{\frac{(1+\bar{a}')(m+\bar{a}')}{2m(1+m)}}\right] \qquad (B.3)$$

where

$$\bar{a}' = \frac{\beta y}{x_{TIP}-(y_{TIP}-y)\beta} = \begin{pmatrix}\text{Value of "a" along the tip} \\ \text{Mach line at span station y}\end{pmatrix}$$

For a supersonic leading edge, $m > 1.0$, the lift distribution behind the tip Mach line is given as

$$\frac{\Delta p(\bar{a})}{q} = \left(\frac{\Delta p(\bar{a})}{q}\right)_{DELTA} \left(\frac{2}{\pi} \sin^{-1}\sqrt{\bar{a}''}\right) \qquad (B.4)$$

where

$\left(\frac{\Delta p(\bar{a})}{q}\right)_{DELTA}$ = Delta wing distribution given by Equation B.2.

$\bar{a}'' = \beta\left(\frac{y_{TIP}-y}{x_{TIP}-x}\right)$ = Value of "$\bar{a}$" relative to forward wing tip.

The functions given above in Equations B.3 and B.4 are exact shapes as required by conical flow theory. Hence, the approximation is still off in overall magnitude only.

A final correction to the delta wing distribution is the subsonic trailing edge term. This term is approximated as a multiplicative function applied to the delta plus tip term. The function is

$$\frac{\Delta p(\bar{a})}{q} = \left(\frac{\Delta p(\bar{a})}{q}\right)_{DELTA+TIP} \left(\frac{2}{\pi} \sin^{-1}\sqrt{\bar{a}'''}\right)$$

for $0.0 \leq \bar{a}''' \leq 1.0$ where

$$\bar{a}''' = \frac{x-x_{TE}}{(x_{TEV}+\beta y)-x_{TE}}$$

$x_{TE} = y\left(\tan \Lambda_{TE}\right) + x_{TEV}$ = x position of trailing edge

x_{TEV} = x position of the trailing edge vertex

thus

$$\bar{a}''' = \frac{y-(x-x_{TEV})\frac{m'}{\beta}}{y(1-m')}$$

$$m' = \frac{\beta}{\tan \Lambda_{TE}} < 1.0$$

The form of this approximation is not exactly correct, however, it seems to be close enough for practical purposes as experience has shown.

Two examples are shown in Figure 22 of the supersonic weighting function. The first example is for a rectangular wing, AR=2.0, in steady flow at M_∞=1.2 and α=1.0 Rad. The solid line is the weighting function simply computed at the span stations η=0.1,0.5 and 0.9 with the equations given

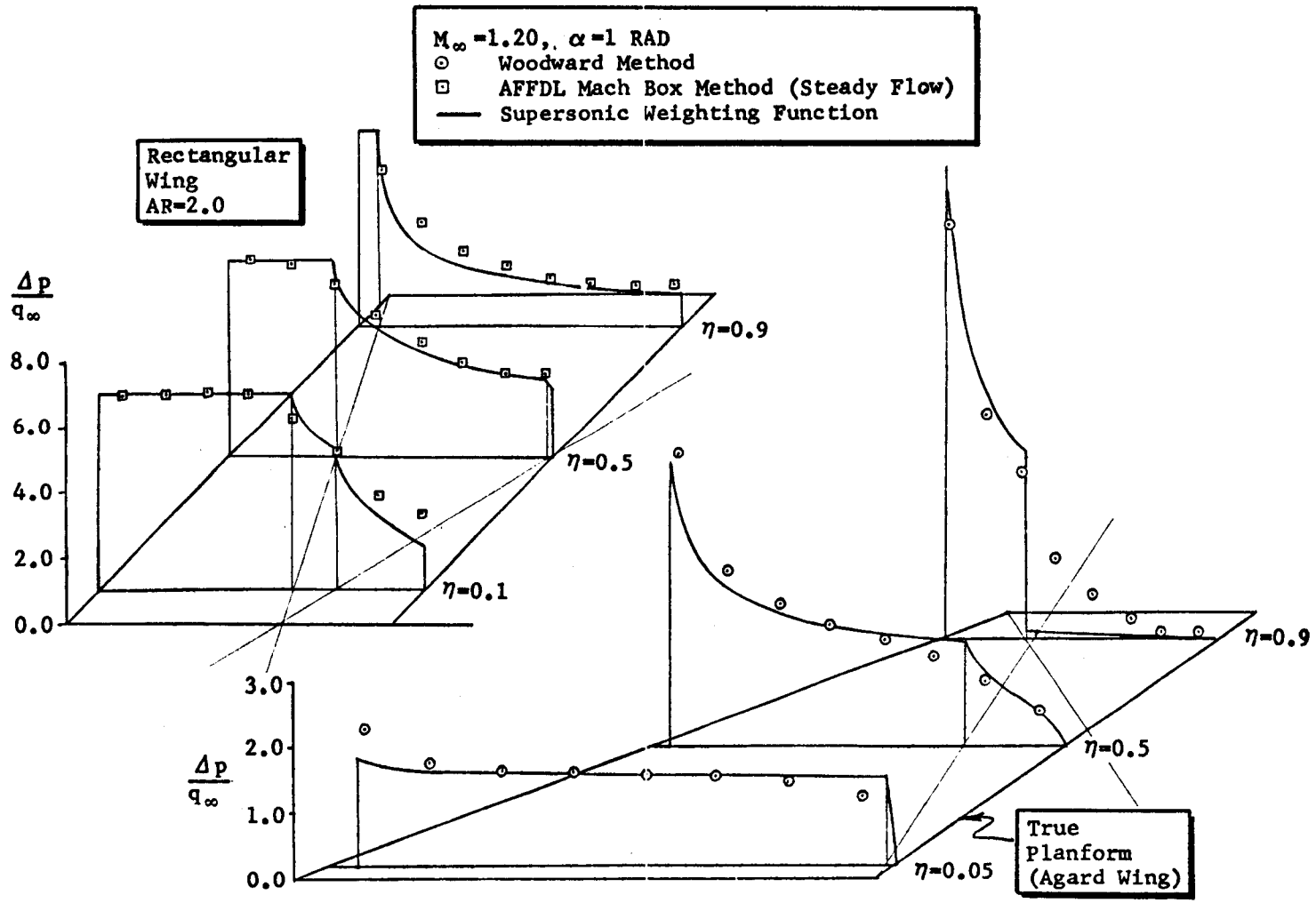

Figure 22 EXAMPLES OF THE SUPERSONIC WEIGHTING FUNCTION

in this appendix. The Mach lines are shown for clarity. The symbols are values computed by the AFFDL Mach box program for wing-tail configurations.[20] In this case, the approximation for the elliptic integral is adequate. The second example is a swept tapered wing of the standard AGARD wing-tail configuration (the true planform is shown). The conditions are steady flow, M_∞ =1.2 and α=1.0 rad. The solid line is again the weighting function but this time a uniform multiplier has been applied to account for the error introduced by the elliptic integral approximation. The symbols are results from the Woodward finite element method.[18] The disagreement at the Mach line discontinuities is due to the inability of the finite element representation to conform to such characteristics with a reasonable number of elements.

The supersonic weighting function was incorporated only into the steady supersonic aerodynamic subroutine. The primary reason was that the use of different functions for supersonic flow further complicated the transonic calculations. Thus, for the purpose of the feasibility study, applications of the weighting function were pursued in steady flow only in order to assess its value to the transonic problem.

An example of some preliminary results is shown in Figure 23. In this case, the standard AGARD wing-tail configuration is considered in steady $M_\infty = 1.2$ flow with both wing and tail at $\alpha = 1.0$ rad. Again, the symbols are the results predicted by the Woodward program. Two collocation solutions are shown. The solid line is the supersonic method with the special weighting function. The dashed line is the original method which is identical to that currently used in the unsteady portion of the program. The disagreement at the root is due to some error in the supersonic weighting function program whose effects apparently disappear in the more outboard sections. This error is also believed to be responsible for low pressures on the tail. The solution with the regular functions shows the usual oscillations about the Woodward solution but seems to be adequate on the wing. The tail pressures are somewhat lower than Woodward. This is the same characteristic that was exhibited in subsonic flow for the same configuration in Figure 19. Thus, it is felt that the difference between subsonic and supersonic flow has been properly predicted with the original method and that the supersonic weighting function program is affected only by a programming error, most likely in the kernel function-pressure function integration for control points near the root.

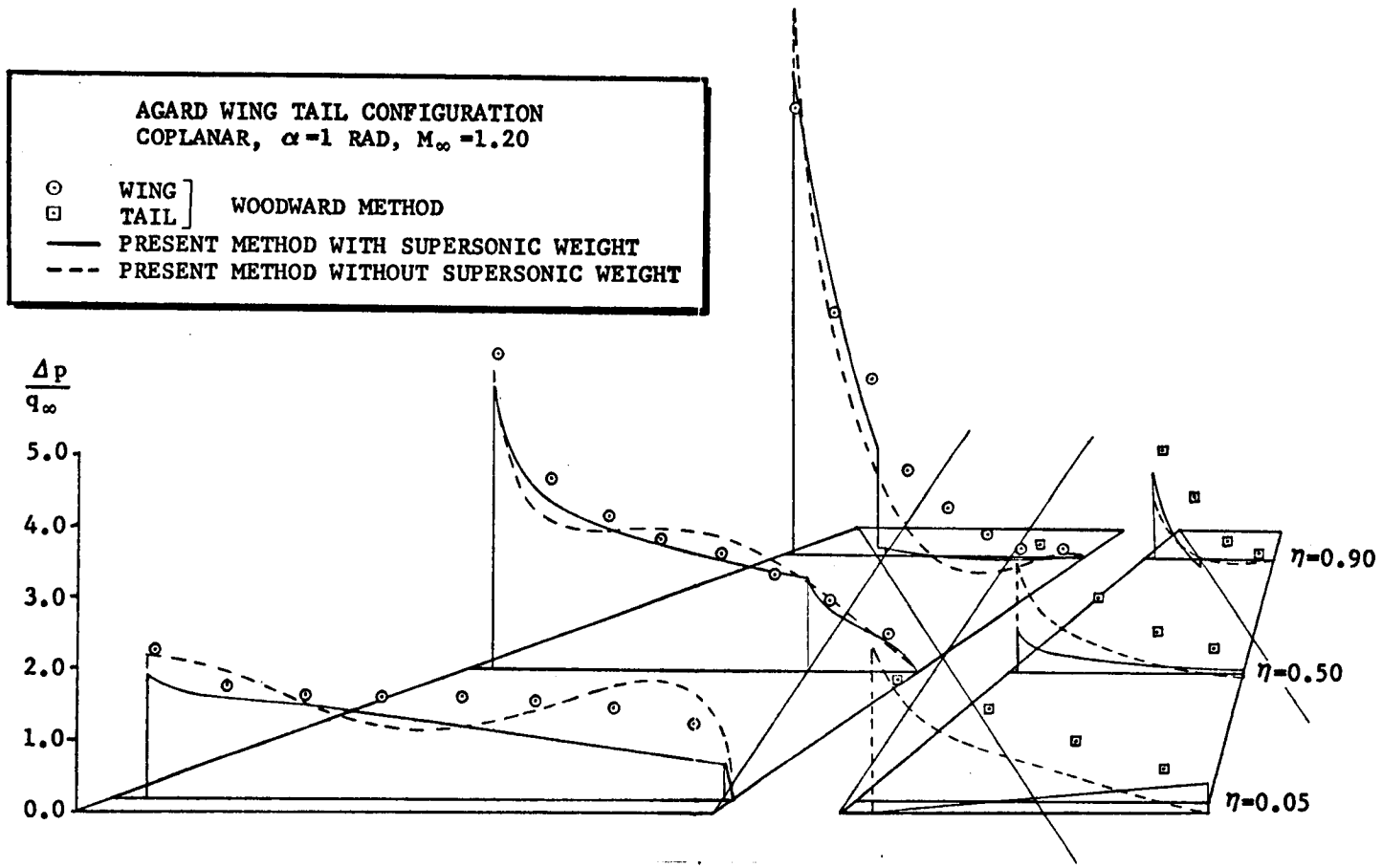

Figure 23 PREDICTED RESULTS FOR A WING-TAIL CONFIGURATION IN STEADY SUPERSONIC FLOW

Unsteady Supersonic Flow and the Non Planar Kernel Function

In the development of the subroutine for computing oscillatory supersonic aerodynamics on interfering surfaces, a peculiarity of the supersonic non-planar kernel function was discovered. The kernel function used is a streamlined version of that presented by Harder and Rodden[22] which is given in Appendix C. The characteristic was not evident in steady flow due to the fact that initial applications were to the AGARD wing-tail configuration for the coplanar case. It was first detected in the non-coplanar case which is described as follows.

A problem was selected for verifying the unsteady supersonic collocation method by comparison with a solution obtained with the AFFDL Mach Box Method. The case was a non-coplanar wing-tail configuration in M_∞ =1.2 flow for k_∞ =0.20 with a unit wing translation mode. The tail was stationary. Both the wing and tail were rectangular, AR=2.0, surfaces with a semi-span of 1.0. The tail leading edge was 0.2 aft and 0.4 above the wing trailing edge. As a result, the Mach hyperbola on the wing for control points near the tail leading edge was forward of the wing trailing edge.

A comparison with the AFFDL Mach box is shown in Figure 24. The number of downwash points used is NC=6 and NS=4 on both the wing and tail for a total of 48 downwash points. The Mach box solution had a total of 80 boxes on the wing and tail plus 109 boxes in the diaphragms. The present method is slightly low toward the wing leading edge for the real part, but shows very good agreement elsewhere on the wing. The disagreement on the tail is a result of the peculiarity in the supersonic kernel function.

In the derivation of the non-planar supersonic kernel function based on the acceleration potential, Harder and Rodden[22] performed the differentiation to obtain the downwash at the control point prior to integration of the kernel function-pressure function product as is normally done in deriving the acceleration potential kernel function. This resulted in a (3/2) power singularity along the Mach hyperbola on any surface that was non-coplanar with the control point. Such a singularity cannot be integrated and the original derivation provided no means for defining a finite part of the improper integral. Since the Woodward method did not have any such problem, it was decided to investigate the taking of the derivative to obtain the downwash since in Woodward's method, the derivative is taken after the integration.

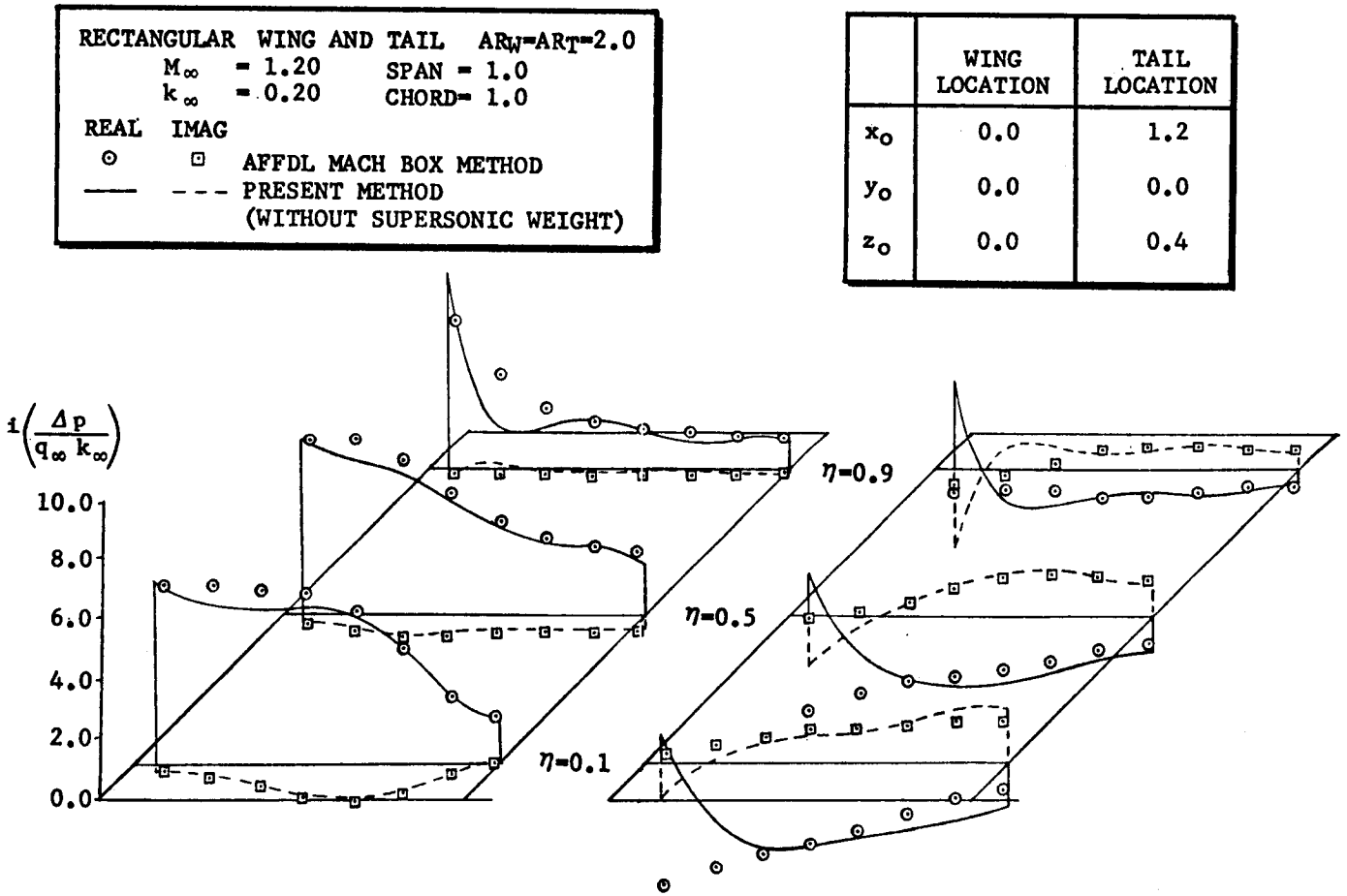

Figure 24 PREDICTED RESULTS ON A NON COPLANAR WING-TAIL CONFIGURATION IN UNSTEADY SUPERSONIC FLOW

By Leibnitz's Rule, it was found that some extra terms were obtained if one differentiated prior to integration. These terms resulted from the fact that if the aft boundary of integration is defined by the Mach hyperbola, it is a function of the variable of differentiation. This does not occur in the coplanar case. One of the extra terms canceled the integrated singularity and hence established the finite part of the improper integral. The other terms were not so strong, and for most cases should have negligible effect.

Since the current program does not require the non-coplanar capability for investigating the transonic algorithm, the only effort that was made toward solving this problem was its definition and the derivation of the method for solution. These results are summarized in Appendix D. The solution shown in Figure 24 illustrates the effect of the (3/2) singularity near the leading edge of the tail. Away from the leading edge, however, the solution approaches the Mach box results. The slight discrepancy near the trailing edge is actually due to the erroneous peak at the leading edge of the tail and is hence of no concern. Thus, it was felt that the supersonic unsteady method for coplanar interference was working properly.

APPENDIX C

THE STEADY AND UNSTEADY NONPLANAR SUPERSONIC KERNEL FUNCTION

Harder and Rodden[22] have presented a nonplanar supersonic kernel function in a form similar to that given earlier by Landahl for subsonic flow.[23] The basic equation is identical for subsonic and supersonic flow and is expressed as

$$K = -\frac{e^{-ikx_o}}{r^2}\left(K_1T_1 + \frac{K_2T_2}{r^2}\right), \quad x_o \geq Br$$

$$K = 0 \qquad , \quad x_o < Br \qquad \text{(C.1)}$$

where

$$T_1 = \cos(\theta_r - \theta_s) \qquad \text{(C.2)}$$

$$T_2 = \left(z_o\cos\theta_r - y_o\sin\theta_r\right)\left(z_o\cos\theta_s - y_o\sin\theta_s\right) \qquad \text{(C.3)}$$

$$r^2 = y_o^2 + z_o^2 \qquad \text{(C.4a)}$$

$$R^2 = x_o^2 - B^2r^2 \qquad \text{(C.4b)}$$

$$x_o, y_o, z_o = \frac{x-\xi}{b_{REF}}, \frac{y-\eta}{b_{REF}}, \frac{z-\zeta}{b_{REF}} \qquad \text{(C.5)}$$

$$k = \frac{b_{REF}}{U} : \quad b_{REF} = \text{Reference Length} \qquad \text{(C.6)}$$

$$B = M^2-1 \qquad \text{(C.7)}$$

The coordinates x_o, y_o, z_o are the non-dimensional distances between the sending (pressure) point at (ξ, η , ζ) and the receiving (downwash) point at (x,y,z). The angles θ_r and θ_s are likewise the inclination of the sending and receiving surfaces relative to the x-y plane.

The K_1 and K_2 terms are quite complex and are given in Reference 22 as

$$K_1 = -\frac{Mr^2}{R}\left[\frac{e^{-ikru_2}}{(1+u_2^2)^{1/2}} + \frac{e^{-ikru_1}}{(1+u_1^2)^{1/2}}\right] - I_1 \tag{C.8}$$

$$K_2 = \left\{\frac{Mr}{R(1+u_2^2)^{3/2}}\left[2 - \frac{B^2(1+u_2^2)r^2}{R^2} - \frac{Mru_2}{R}\right] - \frac{iM^2r^3k}{R^2(1+u_2^2)^{1/2}}\right\} e^{-ikru_2}$$

$$+ \left\{\frac{Mr}{R(1+u_1^2)^{3/2}}\left[2 - \frac{B^2(1+u_1^2)r^2}{R^2} + \frac{Mru_1}{R}\right] + \frac{iM^2r^3k}{R^2(1+u_1^2)^{1/2}}\right\} e^{-ikru_1} + 3I_2 \tag{C.9}$$

where

$$\left.\begin{aligned} u_1 &= \frac{x_o-MR}{B^2r} = -\frac{x_o-MR}{\beta^2 r} \\ u_2 &= \frac{x_o+MR}{B^2r} = -\frac{x_o+MR}{\beta^2 r} \end{aligned}\right\} \beta^2 = 1-M^2 = -B^2 \tag{C.10}$$

and

$$I_1 = \int_{u_1}^{u_2} \frac{e^{-ikru}}{(1+u^2)^{3/2}}\, du \tag{C.11}$$

$$I_2 = \int_{u_1}^{u_2} \frac{e^{-ikru}}{(1+u^2)^{5/2}}\, du \tag{C.12}$$

Through some algebraic manipulations, it is possible to simplify the above set of equations.

The result of simplification in steady flow yields the following expression

$$K_{STEADY} = -\frac{2x_o}{r^2 R}\left[T_1 - T_2\left(\frac{2}{r^2} - \frac{B^2}{R^2}\right)\right] \qquad (C.13)$$

which contains a singularity of strength

$$\lim_{\epsilon \to 0} \left(\frac{1}{\epsilon^{3/2}}\right) \qquad (C.14)$$

as $R \to 0$ along the Mach cone boundary. This singularity cannot be integrated for the nonplanar case but does not appear for coplanar configurations. The finite part of the improper integral of the singularity does exist, however, which is discussed in Appendix D.

The final form of the kernel function in unsteady flow is not as simple as it is for steady flow, yet it is more convenient than that given in Reference 22. The following expressions for K_1 are used in Equation C.1.

$$K_1 = K_{11} + K_{12} \qquad (C.15)$$

where

$$K_{11} = \left[\left(\frac{x_o}{R} + 1\right) - I_{11}\right] e^{-ikru_1} \qquad (C.16a)$$

$$K_{12} = \left[\left(\frac{x_o}{R} - 1\right) + I_{12}\right] e^{-ikru_2} \qquad (C.16b)$$

For $u_1 \geq 0$,

$$I_{11} = ikre^{-ikru_1} \sum_{n=1}^{11} \frac{a_n E_1^n}{nc+ikr} \qquad \text{(C.17a)}$$

or for $u_1 < 0$,

$$I_{11} = ikre^{-ikru_1} \sum_{n=1}^{11} \frac{a_n E_1^n}{nc-ikr}$$

$$+ 2\left[e^{-ikru_1} - 1 + (kr)^2 \sum_{n=1}^{11} \frac{a_n}{(nc)^2+(kr)^2}\right] \qquad \text{(C.17b)}$$

and

$$I_{12} = ikre^{-ikru_2} \sum_{n=1}^{11} \frac{a_n E_2^n}{nc+ikr} \qquad \text{(C.17c)}$$

where

$$\left.\begin{aligned} E_1 &= e^{-c|u_1|} \\ E_2 &= e^{-cu_2} \end{aligned}\right\} c = 0.372 \qquad \begin{matrix} \text{(C.17d)} \\ \text{(C.17e)} \end{matrix}$$

For the K_2 term, the following expressions are used in Equation C.1

$$K_2 = K_{21} + K_{22} \qquad \text{(C.18)}$$

where

$$K_{21} = 3I_{11} - I_{21} - \left\{2\left(\frac{x_o}{R}+1\right) - \frac{r^2}{R^2}\left[\frac{B^2 x_o}{R} - \frac{ikrM^2}{(1+u_1^2)^{1/2}}\right]\right\} e^{-ikru_1} \qquad \text{(C.19a)}$$

$$K_{22} = -3I_{12} + I_{22} - \left\{2\left(\frac{x_o}{R}-1\right) - \frac{r^2}{R^2}\left[\frac{B^2 x_o}{R} + \frac{ikrM^2}{(1+u_2^2)^{1/2}}\right]\right\} e^{-ikru_2} \qquad \text{(C.19b)}$$

For $u_1 \geq 0$,

$$I_{21} = ikre^{-ikru_1} \sum_{n=1}^{11} \frac{b_n E_1^{2n}}{2nc+ikr} \qquad \text{(C.20a)}$$

or for $u_1 < 0$,

$$I_{21} = ikre^{-ikru_1} \sum_{n=1}^{11} \frac{b_n E_1^{2n}}{2nc-ikr}$$

$$+ 2\left[e^{-ikru_1} - 1 + (kr)^2 \sum_{n=1}^{11} \frac{b_n}{(2nc)^2+(kr)^2} \right] \qquad \text{(C.20b)}$$

and

$$I_{22} = ikre^{-ikru_2} \sum_{n=1}^{11} \frac{b_n E_2^{2n}}{2nc+ikr} \qquad \text{(C.20c)}$$

The a_n and b_n coefficients in the series summations in Equations C.17 and C.20 are given in Table C.1. The a_n set are those given originally by Laschka[24] for the approximation

$$\left(\frac{u}{(1+u^2)^{1/2}} - 1 \right) \approx \sum_{n=1}^{11} a_n e^{-ncu} \qquad \text{(C.21a)}$$

The b_n set are those given by Cunningham[1] for the approximation

$$\left(\frac{u^3}{(1+u^2)^{3/2}} - 1 \right) \approx \sum_{n=1}^{11} b_n e^{-ncu} \qquad \text{(C.21b)}$$

Table C.1

n	a_n	b_n
1	-0.24186198	-3.509407
2	2.7968027	57.17120
3	-24.991079	-624,7548
4	111.59196	3830.151
5	-271.43549	-14538.51
6	305.75288	35718.32
7	41.183630	-57824.14
8	-545.98537	61303.92
9	644.78155	-40969.58
10	-328.72755	15660.04
11	64.279511	-2610.093

APPENDIX D

TREATMENT OF THE IMPROPER INTEGRAL OF THE NONPLANAR SUPERSONIC KERNEL FUNCTION

The potential at point x, y, z for a supersonic doublet due to a pressure difference Δp at ξ, η, ζ directed in the positive z, ζ direction, is as follows:

$$\phi(x, \xi, y, \eta, z, \zeta) = - \frac{\Delta p U}{4 \pi \rho} \frac{z_o x_o D(x_o - Br)}{r^2 R} \tag{D.1}$$

where all terms are as defined previously and

$$D(x_o - Br) = \begin{bmatrix} 1, & x_o \geq Br \\ 0, & x_o < Br \end{bmatrix}$$

The total potential at (x,y,z) due to a surface, S, of constant Δp distribution is the integral over S as follows:

$$\phi(x,y,z) = - \frac{\Delta p U}{4 \pi \rho} \iint_S \frac{z_o x_o D(x_o - Br)}{r^2 R} \, d\xi \, d\eta \tag{D.2}$$

The downwash in the z direction at point (x,y,z) is then

$$w(x,y,z) = \frac{\partial}{\partial z} \phi \, (x,y,z) \tag{D.3}$$

The Woodward method[18] uses this sequence of operations where differentiation at the downwash point is performed after integration of the total potential.

In the kernel function formulation, following Harder and Rodden[22] and Landahl[23], differentiation is performed before integration. The interchange is permissible as long as the limits of integration are not a function of the variable of differentiation, which in this case is z. For subsonic flow,

the integration limits are defined completely by planform boundary. In supersonic flow for coplanar surfaces, the limits are defined by planform and the forward Mach cone whose location is independent of z. For nonplanar configurations in supersonic flow the boundary is again defined as for the coplanar case, however, the Mach cone boundary is now a hyperbola whose location is a function of z for a fixed ζ.

Leibnitz's rule for differentiating an integral with respect to a parameter is as follows:

$$\frac{d}{dt}\int_{a(t)}^{b(t)} g(x,t)dx = g\left[b(t),t\right]\frac{\partial b(t)}{\partial t}$$

$$-g\left[a(t),t\right]\frac{\partial a(t)}{\partial t} + \int_{a(t)}^{b(t)} \frac{\partial}{\partial t}\left[g(x,t)\right] dx \qquad (D.4)$$

The limits a(t) and b(t) are constant in subsonic and coplanar supersonic flow; thus, their derivatives are zero. For the noncoplanar case the derivatives must be accounted for. Starting with the double integral for w(x,y,z), we have

$$\frac{\partial}{\partial z}\phi(x,y,z) = \frac{\partial}{\partial z}\int_{\eta_1}^{\eta_2}\int_{\xi_{LE}}^{\xi_{mc}} \phi(x,\xi,y,\eta,z,\zeta)d\xi\, d\eta \qquad (D.5)$$

where η_1 and η_2 are the spanwise limits defined by the Mach

cone intersection with the planform boundary. The limits ξ_{LE} and ξ_{mc} are the leading edge and Mach hyperbola boundaries. Applying Leibnitz's rule to the spanwise integral yields

$$\frac{\partial}{\partial z}\,\phi(x,y,z) = G(x,y,\eta_2,z,\zeta)\,\frac{\partial \eta_2}{\partial z} \tag{D.6}$$

$$-G(x,y,\eta_1,z,\zeta)\,\frac{\partial \eta_1}{\partial z} + \int_{\eta_1}^{\eta_2} \frac{\partial}{\partial z} \int_{\xi_{LE}}^{\xi_{mc}} \phi(x,\xi,y,r,z,\zeta)\,d\xi\,d\eta$$

where

$$G(x,y,\eta,z,\zeta) = \int_{\xi_{LE}}^{\xi_{mc}} \phi(x,\xi,y,\eta,z,\zeta)\,d\xi$$

The inner integral in Equation D.6 also becomes

$$\frac{\partial}{\partial z} \int_{\xi_{LE}}^{\xi_{mc}} \phi(x,\xi,y,\eta,z,\zeta)\,d\xi = \phi(x,\xi_{LE},y,\eta,z,\zeta)\,\frac{\partial \xi_{mc}}{\partial z}$$

$$- \phi(x,\xi_{mc},y,\eta,z,\zeta)\,\frac{\partial \xi_{LE}}{\partial z} + \int_{\xi_{LE}}^{\xi_{mc}} \frac{\partial}{\partial z}\,\phi(x,\xi,y,\eta,z,\zeta)\,d\xi \tag{D.7}$$

In Equations D.6 and D.7, all of the extra terms are nonzero with exception of $\frac{\partial \xi_{LE}}{\partial z}$. When the Mach hyperbola intersects the planform at say a streamwise tip, the corresponding η_1 or η_2 derivative is also zero.

All of the nonzero terms in Equations D.6 and D.7 should be accounted for; however, in most cases the η_1 and η_2 derivatives will contribute very little and may usually be ignored. The stronger term results from $\frac{\partial \xi_{mc}}{\partial z}$ to which we will restrict our discussion. The form of ξ_{mc} is

$$\xi_{mc} = x - Br \tag{D.8}$$

which yields

$$\frac{\partial \xi_{mc}}{\partial z} = \frac{\partial \xi_{mc}}{\partial r} \frac{\partial r}{\partial z} = - \frac{Bz_o}{r}$$

Now, the nonzero derivative term in Equation D.7 becomes

$$\phi(x, \xi_{mc}, y, \eta, z, \zeta) \frac{\partial \xi_{mc}}{\partial z} = \frac{\Delta p U}{4\pi\rho} \frac{Bz_o}{r} \left[\frac{z_o x_o D(x_o - Br)}{r^2 R} \right]_{\xi = \xi_{mc}}$$

but,

$$\frac{z_o x_o}{r^2} \left(\frac{1}{R} \right)_{\xi = \xi_{mc}} = \frac{z_o B}{r} \left(\lim_{\xi \to \xi_{mc}} \frac{1}{R} \right)$$

which is square root singular. Thus, the term becomes

$$\phi(x, \xi_{mc}, y, \eta, z, \zeta) \frac{\partial \xi_{mc}}{\partial z} = \frac{\Delta p U}{4\pi\rho} \frac{B^2 z_o^2}{r^2} \left(\lim_{\xi \to \xi_{mc}} \frac{1}{R} \right) \tag{D.9}$$

The integral in Equation D.7 contains the differentiation inside the integral sign, thus

$$\int_{\xi_{LE}}^{\xi_{mc}} \frac{\partial}{\partial z} \phi(x, \xi, y, \eta, z, \zeta) d\xi = - \frac{\Delta p U}{4\pi\rho} \int_{\xi_{LE}}^{\xi_{mc}} \frac{\partial}{\partial z} \left[\frac{x_o z_o D(x_o - Br)}{r^2 R} \right] d\xi$$

but

$$\frac{\partial}{\partial z} \left[\frac{z_o x_o D(x_o - Br)}{r^2 R} \right] = \frac{x_o}{r2R} \left[1 - \frac{2z_o^2}{r^2} + \frac{z_o^2 B^2}{R^2} \right] \qquad (D.10)$$

thus

$$\int_{\xi_{LE}}^{\xi_{mc}} \frac{\partial}{\partial z} \phi(x, \xi, y, \eta, z, \zeta) d\xi =$$

$$- \frac{\Delta p U}{4\pi\rho} \int_{\xi_{LE}}^{\xi_{mc}} \frac{x_o}{r2R} \left[1 - \frac{2z_o^2}{r2} + \frac{z_o^2 B^2}{R^2} \right] d\xi \qquad (D.11)$$

which contains the improper integral

$$I_s = - \frac{\Delta p U}{4\pi\rho} \int_{\xi_{LE}}^{\xi_{mc}} \frac{x_o z_o^2 B^2}{r^2 R^3} d\xi \qquad (D.12)$$

due to the term R^3 as $\xi \rightarrow \xi_{mc}$ which is a 3/2 power singularity. Evaluating I_s gives

$$I_s = - \frac{\Delta p U}{4\pi\rho} \frac{z_o^2 B^2}{r^2} \left[\left(\underset{\xi \rightarrow \xi_{mc}}{\text{LIM}} \frac{1}{R} \right) - \frac{1}{R_{LE}} \right] \qquad (D.13)$$

Inserting Equations D.9, D.11 and D.13 into Equation D.7, we obtain

$$\frac{\partial}{\partial z}\int_{\xi_{LE}}^{\xi_{mc}} \phi(x,\xi,y,\eta,z,\zeta)d\xi = -\frac{\Delta p U}{4\pi\rho}\left\{\frac{z_o^2 B^2}{r^2}\left[\lim_{\xi\to\xi_{mc}}\left(\frac{1}{R}-\frac{1}{R}\right)\right.\right.$$

$$\left.\left. -\frac{1}{R_{LE}}\right] + \int_{\xi_{LE}}^{\xi_{mc}} \frac{x_o}{r^2 R}\left[1-\frac{2z_o^2}{r^2}\right]d\xi\right\},$$

which becomes

$$\frac{\partial}{\partial z}\int_{\xi_{LE}}^{\xi_{mc}} \phi(x,\xi,y,\eta,z,\zeta)d\xi =$$

$$-\frac{\Delta p U}{4\pi\rho}\left\{\frac{z_o^2 B^2}{r^2 R_{LE}} + \int_{\xi_{LE}}^{\xi_{mc}} \frac{x_o}{r^2 R}\left[1-\frac{2z_o^2}{r^2}\right]d\xi\right. \qquad \text{(D.14)}$$

The extension of Equation D.14 to nonparallel surfaces and unsteady flow follows along the same path of logic. For the more general case where Δp is a function of ξ and η, the value used in Equations D.9 and D.13 for Δp is $\Delta p(\xi_{mc},\eta)$.

NASA CR-112264
DISTRIBUTION LIST
NAS1-11565

	No. Copies
NASA Langley Research Center Hampton, VA 23365	
Attn: Report & Manuscript Control Office, Mail Stop 180A	1
Raymond L. Zavasky, Mail Stop 115	1
Robert N. Desmarais, Mail Stop 340	20
Loads Division, Mail Stop 242	2
Aeroelasticity Branch, Mail Stop 340	1
NASA Ames Research Center Moffett Field, CA 94035	
Attn: Library, Mail Stop 202-3	1
Dr. Harvard Lomax, Mail Stop 233-1	2
NASA Flight Research Center P. O. Box 273 Edwards, CA 93523	
Attn: Library	1
NASA Goddard Space Flight Center Greenbelt, MD 20771	
Attn: Library	1
NASA Manned Spacecraft Center 2101 Webster Seabrook Road Houston, TX 70058	
Attn: Library, Code JM6	1
NASA Marshall Space Flight Center Huntsville, AL 35812	
Attn: Library	1
Jet Propulsion Laboratory 4800 Oak Grove Drive Pasadena, CA 91103	
Attn: Library, Mail 111-113	1
NASA Lewis Research Center 21000 Brookpark Road Cleveland, OH 44135	
Attn: Library, Mail Stop 60-3	1

NASA CR-112264
DISTRIBUTION LIST
NAS1-11565

	No. Copies
NASA John F. Kennedy Space Center Kennedy Space Center, FL 32899 Attn: Library, IS-DOC-12L	1
National Aeronautics & Space Administration Washington, DC 20546 Attn: KSS-10/Library RW/NASA Headquarters	1 1
The Boeing Company Commercial Airplane Group P. O. Box 3707 Seattle, WA 98124 Attn: Dr. Wes Howard, Mail Stop 77-06	2
Nielsen Engineering & Research, Inc. 850 Maude Avenue Mountain View, CA 94040 Attn: Dr. Stephen S. Stahara	2
Lockheed California Company Dept. 7433 Bldg. 243, Plant 2 Burbank, CA 91503 Attn: Dr. James D. Revell	2
The University of Tennessee Space Institute Tullahoma, TN 37388 Attn: Dr. J. M. Wu	1
Air Force Flight Dynamics Laboratory Wright-Patterson Air Force Base, OH 45433 Attn: Walter J. Mykytow, Vehicle Dynamics Division James J. Olsen	2 2
NASA Scientific & Technical Information Facility P. O. Box 33 College Park, MD 20740	11 plus reproducible
Illinois Institute of Technology MMAE Chicago, IL 60616 Attn: Dr. E. Albano	1